We are IntechOpen,
the world's leading publisher of
Open Access books
Built by scientists, for scientists

4,800
Open access books available

122,000
International authors and editors

135M
Downloads

Our authors are among the

154
Countries delivered to

TOP 1%
most cited scientists

12.2%
Contributors from top 500 universities

CLARIVATE ANALYTICS
BOOK CITATION INDEX
INDEXED

WEB OF SCIENCE™

Selection of our books indexed in the Book Citation Index
in Web of Science™ Core Collection (BKCI)

Interested in publishing with us?
Contact book.department@intechopen.com

Numbers displayed above are based on latest data collected.
For more information visit www.intechopen.com

Adiabatic Shear: Pre- and Post-critical Dynamic Plasticity Modelling and Study of Impact Penetration. Heat Generation in this Context

Patrice Longère[1] and André Dragon[2]
[1]Université Européenne de Bretagne (UBS, LIMATB)
[2]Laboratoire de Mécanique et de Physique des Matériaux (CNRS, ENSMA)
France

1. Introduction

Adiabatic Shear Banding (ASB) is recognized as a phenomenon of notable importance, being a failure precursor in the context of dynamic deformation for a large class of metals and alloys (in particular high-strength steels and alloys) and non-metals (polymers). Stemming from the pioneering work of Zener & Hollomon (1944), Recht (1964), extensive investigation – metallurgical and mechanical, experimental and theoretical –, and relevant literature have been devoted to the matter, see for instance numerous references given in the books by Bai & Dodd (1992), Wright (2002). These authors have attempted complementary syntheses of the field ranging from materials science oriented research to non linear mechanics issues. The special issue 'Shear Instabilities and Viscoplasticity Theories' of Mechanics of Materials published in 1994, including notably the papers by Mason et al. (1994), Nemat-Nasser et al. (1994), keeps also its topical importance. The seminal contribution by Marchand & Duffy (1988) should be cited as a major experimental work.

The emergence of ASB is attributed predominantly to the opposite influence of strain and strain rate hardening and thermal softening effects, respectively. Thermal softening is assumed to lead to a stage when the material can no longer harden and, in this way, looses its stability, making possible the formation of a localized discontinuity/failure mode. This is why many studies of instability inception are concerned, in this context, with perturbation analysis of the mechanical and thermal fields, see for instance Molinari & Clifton (1987). Very recent results regarding the ASB phenomenon bring out some finer points to the picture mentioned above. They tend to clarify the role of microstructural evolutions and point out a particular phase transition, namely dynamic recrystallization as a possible factor in the ASB generation (Rittel et al., 2008). Adiabatic shear mode requires that thermal conductivity effects be attenuated by a small deformation time, i.e. high strain rate involved. In such a way this mode is considered sometimes as 'a characteristics' of impact loading (Woodward, 1990).

Depending on the thermomechanical properties of the target material and on the intensity of loading, the penetration of a flat end projectile into, say, a hard steel plate can be accompanied by the formation of a ring shape intense (localized) shear zone inside the target. Intense shearing can lead to the development of adiabatic shear bands which are

known as precursor of the ultimate dynamic plugging of the plate. In the present authors' opinion accurate prediction of the protection response during the target/penetrator interaction needs an advanced three-dimensional (3D) description of the behaviour of the structural materials containing adiabatic shear bands. The 3D TEVPD (for Thermo Elastic ViscoPlastic with Viscous Deterioration) constitutive model and the inherent numerical formalism, presented in this chapter, aim to describe the post-critical behaviour of a high strength metallic material in the presence of the ASB related evolution.

In the approach presented, ASB is considered as a specific anisotropic deterioration process. Some earlier tentatives in this direction are due to Pecherski (1988), and Perzyna and coworkers, see e.g. Perzyna (1990). The constitutive model presented here describes the thermo-elastic/viscoplastic behaviour of a sound material and the mechanical anisotropy, i.e. directional degradation of both elastic and viscoplastic moduli, induced by ASB in the framework of large elastic-plastic deformation. The model, particularly destined to deal with impacted structures, has been progressively elaborated in recent articles (Longère et al., 2003; 2005; 2009). It is applied to a genuine ballistic penetration problem for a target plate material, namely to the interaction between a fragment simulating projectile (FSP) and a semi-thick target metal plate.

Since thermal evolutions are crucial in the ASB related research, special importance has been given to the real-time monitoring of the temperature of impacted specimens, see e.g. Mason et al. (1994), Kapoor & Nemat-Nasser (1998), Rittel (1999), Rosakis et al. (2000). These works have led to a better understanding of the thermomechanical conversion phenomena, notably to the fraction of the plastic work rate converted into heat, corresponding to inherent dissipative nature of plastic deformation. Despite of widespread, crude practice assuming the inelastic heat fraction coefficient as a constant, there is now experimental evidence that it is not only strain but also strain-rate and possibly temperature dependent quantity. Based on this experimental work and some earlier modelling tentatives (Aravas et al., 1990; Zehnder, 1991; Rosakis et al., 2000), some present authors' recent contributions to the matter of the adiabatic heat evaluation viewed as an evolving process are synthesized in this chapter. It can be shown that the accuracy in the prediction of favourable conditions for the onset of plastic (ASB) localization is dependent strongly on the method retained for evaluating the fraction of effectively dissipated plastic work (i.e. converted into heat), see e.g. Longère & Dragon, 2009. Moreover, a methodology combining some aspects of dislocation theory in the domain of thermally activated deformation and the internal variable approach applied to thermo-elastic/viscoplastic behaviour is developed (Voyiadjis & Abed, 2006; Longère & Dragon, 2008); it allows for obtaining physically based inelastic heat fraction expressions. This contribution is summarized at the end of the chapter.

In such a way this chapter brings forward a threefold contribution relevant to the ASB process as a part of dynamic plasticity of high strength metallic materials. It is organized as follows:

i.   A three-dimensional finite deformation model is first presented; the model is based on a specific scale postulate and devoted to cover a wide range of dissipative phenomena including ASB related material instabilities i.e. strong softening prefailure stage. The model and related indicator of the ASB onset are reviewed in Section 2.

ii.   A ballistic penetration problem representing the dynamic interaction between an FSB-projectile and a target plate is rehearsed in Section 3. The three-dimensional numerical study shows the failure of the target occurring as a plugging event resulting from an adiabatic shearing process.

iii. An evaluation of the inelastic heat fraction under adiabatic conditions involving microstructure supported dynamic plasticity modelling is discussed in Section 4 in relation to the dynamic plastic (ASB) localization.

As an introduction to a very recent lecture on adiabatic shear localization, Rittel (Rittel, 2009) pointed out that 'so far, there is no clear connection between the profusion of microstructural observations and mechanical quantities, such as a critical strain for failure, so that the physical picture is still incomplete'. This chapter, summarizing some recent contributions of the authors to the field, embodied in the (i), (ii) and (iii) foregoing items, attempts to fill the gap regarding 'mechanical quantities', i.e. strictly speaking the thermomechanical insight into the 'physical picture' of ASB phenomenon and its salient engineering aspects.

2. Finite strain viscoplasticity model incorporating ASB-induced degradation

2.1 Context and basic concepts

In some engineering applications, notably those implying detailed analysis of consecutive phases for impacted metallic structures (see e.g. Stevens & Batra, 1998, Martinez et al., 2007) and high speed machining (see e.g. Molinari et al., 2002, Burns & Davies, 2002) with the predominant failure mechanism triggered by adiabatic shear banding (ASB), a three-dimensional insight and treatment are desirable. They are scarce in the literature as the relative modelling should be rigorous enough and robust as well to incorporate and overcome local instabilities relative to inception and growth of ASB. Contrarily to fine, micromechanical and one-dimensional analyses encountered in many valuable studies (Bai (1982), Clifton et al. (1984), Molinari (1985,1997) and Klepaczko (1994)) what is searched here, in the context mentioned in the foregoing, is a 'larger scale' material response to dynamic loading. Some attempts by Perzyna and coworkers (see e.g. Perzyna (1990), Lodygowski & Perzyna (1997)) are directed towards such an alternative large-scale, three-dimensional modelling. The aim of the present contribution is clearly set in this perspective. The approach proposed is a phenomenological one – while many hypotheses are micromechanically motivated –, however the model outlined is not a micromechanical model strictly speaking. It is based on the choice of the reference representative volume element (RVE) whose length scale is much greater than the bandwidth (while many existing works, some of them cited above, consider in fact a length scale lower than the bandwidth). An approach accounting for salient physical features concerning the ASB formation and development at the actual (global) RVE scale, should obviously consider the following consequences:

• thermo-mechanical softening;
• ASB-induced material anisotropy (due to band orientation);
• specific finite strain kinematics including ASB-effect.

In the approach put forward, the evolution of the 'singular' dissipative processes (intervening inside the band cluster), contributing to macromechanical (global) softening is described via the evolution of a single internal variable, called ASB-intensity d. The softening behaviour, see e.g. its detailed analysis by Marchand & Duffy (1988) and Liao & Duffy (1998), is being considered as resulting from ASB-induced degradation, the density d characterises the state of the global material deterioration due to ASB as shown in Fig.1.
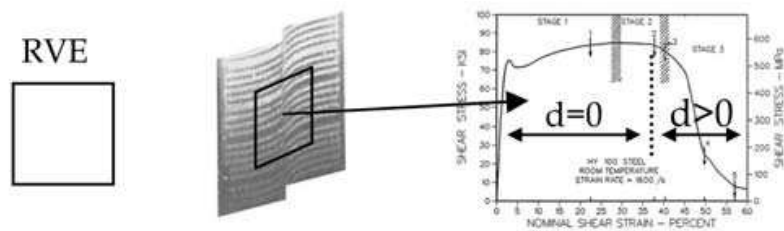
Fig. 1. 'Large RVE' concept illustrated by Marchand and Duffy dynamic torsion experiment and consecutive global softening corresponding to growing density d according to the present model

In order to describe the state of anisotropic degradation of the material caused by the presence of ASB, a second order tensor, damage-like variable **D** is introduced. Its components are denoted as D_{ij} and are expressed by Eq.(1) below, where d^α and $\mathbf{n}^\alpha$ represent respectively the scalar density introduced above and the orientation for the band pattern α, see Fig.2.

$$D_{ij} = \sum_\alpha d^\alpha N_{ij}^\alpha \; ; N_{ij}^\alpha = n_i^\alpha n_j^\alpha \tag{1}$$

For a high strain rate plastic flow considered hereby the work done in plastic deformation (intrinsic dissipation) is converted largely to heat. The latter, if not conducted away as it is the case under the conditions at stake, leads to a high rise in temperature. In metals and alloys where the rate of thermal softening (a corresponding drop in stress) surpasses the rate of work hardening, deformation is seen to concentrate in narrow softened bands of adiabatic shear. This is a nowadays well-known mechanism of ASB inception and growth (Zener & Hollomon (1944), Recht (1964)). Consequently in the framework of the present model, the onset and further evolution of ASB are produced by thermal softening, respectively in the sound (non degraded) material during locally homogeneous plastic deformation and then inside the bands themselves, during evolving localization process. The intensity d^α includes thus information relative to temperature inside the band pattern α. Consider now a single band pattern (Fig.2, $\alpha=1$) and recall that the adjective 'singular' applies to the process relevant to the ASB itself (inside the bands), and the adjective 'regular' for the processes outside the bands. With such a distinction, the current density d of the internal variable **D** depends on the 'singular' temperature T*, and can be thus written as:

$$d = d\left(T^*,...\right) \tag{2}$$

The dots represent other possible singular arguments as it is further detailed.

The kinematic consequences of the presence of the shear band pattern (see Fig.2) are viewed as those of a 'super-dislocation' (or a 'super gliding system'). By generalizing, for the RVE-element considered, the kinematics of the crystalline plasticity, an ASB-induced supplementary ('singular') velocity gradient **L**$^\mathbf{d}$ (in addition to the one relevant to 'regular' plastic deformation outside the band, designated **L**$^\mathbf{p}$) is introduced as the result of the glide velocity $\dot{\gamma}^\alpha$ due to the band pattern α of the normal $\mathbf{n}^\alpha$ and with orientation $\mathbf{g}^\alpha$ (see Fig.2):

$$L_{ij}^d \propto \sum_\alpha \dot{\gamma}^\alpha g_i^\alpha n_j^\alpha \tag{3}$$

Adiabatic Shear: Pre- and Post-critical Dynamic Plasticity Modelling
and Study of Impact Penetration. Heat Generation in this Context

237

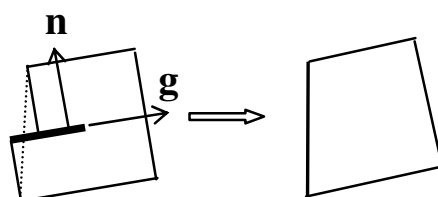
Fig. 2. Equivalent homogeneous volume element containing a family of band (α=1)

The partition of this ASB-induced velocity gradient $\mathbf{L^d}$ into symmetric and antisymmetric parts respectively leads to the corresponding strain rate $\mathbf{d^d}$ and spin $\mathbf{\omega^d}$ as follows:

$$\begin{cases} d_{ij}^{d} \propto \sum_{\alpha} \dot{\gamma}^{\alpha} M_{ij}^{\alpha} \; ; M_{ij}^{\alpha} = \left(g_i^{\alpha} n_j^{\alpha}\right)^{S} = \frac{1}{2}\left(g_i^{\alpha} n_j^{\alpha} + g_j^{\alpha} n_i^{\alpha}\right) \\ \omega_{ij}^{d} \propto \sum_{\alpha} \dot{\gamma}^{\alpha} T_{ij}^{\alpha} \; ; T_{ij}^{\alpha} = \left(g_i^{\alpha} n_j^{\alpha}\right)^{AS} = \frac{1}{2}\left(g_i^{\alpha} n_j^{\alpha} - g_j^{\alpha} n_i^{\alpha}\right) \end{cases} \quad (4)$$

The corresponding kinematics leads to further smoothing of the boundary discontinuity caused by the ASB as illustrated in Fig.2, as it is done in crystalline plasticity. Finally, two contributions to the inelastic strain rate of the equivalent homogeneous volume element can be distinguished: the 'regular' plastic strain rate, denoted $\mathbf{d^p}$, and the 'singular' one, $\mathbf{d^d}$. The total inelastic strain rate $\mathbf{d^{dp}}$ is defined as the sum of these two contributions:

$$d_{ij}^{dp} = d_{ij}^{p} + d_{ij}^{d} \quad (5)$$

The physical motivations and scale assumptions put forward in the foregoing are further developed in Sect.2.2. The complete constitutive model is given in Sect.2.3 in the specific three-dimensional, finite strain, elastic/viscoplastic and ASB-anisotropic degradation framework. The regular vs. singular dissipation terms are respectively designated and corresponding regular vs. singular heating parts specified.

The specific shock configurations for a hat shape structure (HSS) and ballistic penetration involving plugging failure mechanism have been chosen as examples of the application of the present model. The numerical results relevant to HSS configurations, leading to partial or complete banding (and subsequent failure) depending on the shock intensity, see Longère et al. (2005 and 2009), have been examined and compared with experimental data obtained by Couque (2003)$_{a,b}$. A tentative, ASB-induced local failure criterion is being inferred from the corresponding analysis and experimental evidence. The HSS problem investigation, not detailed in this chapter, was viewed as a stage towards genuine ballistic engineering problems where the ASB trajectories cannot be known a priori.

A particular problem of this kind is being dealt with in Sect.3.2, involving a fragment simulating projectile (FSP) and a semi-thick plate interaction. A three-dimensional numerical study is summarized for shock configurations below and above the ballistic penetration limit velocity V_{bpl}. The thermoelastic/viscoplastic/ASB deterioration model (TEVPD) employed allows for bringing out complex ASB-related history regarding impacted plate material. The history at stake consists in occurrence of two competing ASB deterioration mechanisms. The first one, starting earlier, involves a set of localized bands related potentially to punching failure. However, these bands arrest without crossing the plate thickness. It is shown that a new family of crossing bands appears, leading finally to expected plugging failure pattern.

It should be stressed that the thermomechanical TEVPD model, detailed earlier in Longère et al. (2003;2005), represents a specific, directly applicable alternative with respect to non-local modelling due to its proper scale postulate involving material length. The numerical simulations regarding various shock configurations for initial/boundary value problems are intended to put to the test the pertinence of the TEVPD model as a predictive tool for structural analysis involving shock/impact problems. In a sense they appear conclusive for the model legitimation and prospective improvements.

2.2 Physical motivations

Consider simple shear of a material element shown in Fig.3 (the pictures are due to Marchand & Duffy (1988)). Let us suppose the succession of events as follows implying ASB phenomenon where the last picture shows the near-failure stage (involving neither genuine damage nor fracture yet) of the element under adiabatic shear banding.
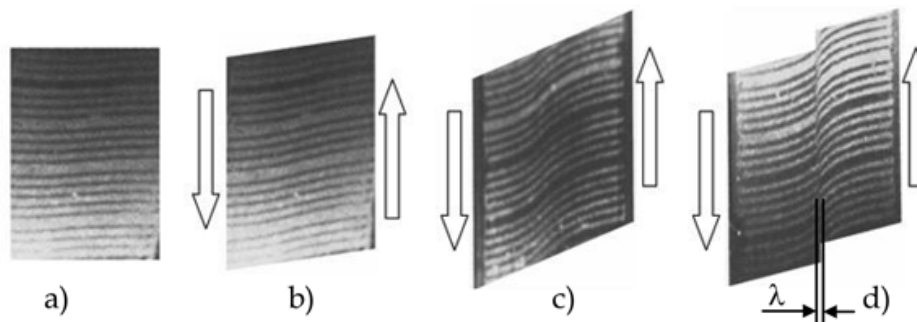

Fig. 3. Material element under dynamic shearing as observed by Marchand & Duffy (1988); a) Undeformed configuration ; b) Homogeneous shear deformation ; c) Weak localization ; d) ASB induced strong localization

The band width is designated λ, and the representative volume element (RVE) is assumed tentatively with a length equal to $\ell < \lambda$. To distinguish the process relevant strictly to the band deformation mechanisms from the process not relevant to the band, the first is henceforth called 'singular' process and the other is called 'regular' one. It is now supposed that the evolution of both processes can be described via the evolution of state variables such like relevant measures of elastic strain $\mathbf{e^e}$, temperature T, strain hardening p, damage (if any) δ, metallurgical state as f.ex. phase transformation (if any) ξ, and so on:

$$V_{regular} = \left(\mathbf{e^e}, T, p, \delta, \xi, ... \right) \text{ and } V_{singular} = \left(\mathbf{e^e}*, T*, p*, \delta*, \xi*, ... \right)$$

where $V_{regular}$ and $V_{singular}$ represent respectively the sets of 'regular' and 'singular' state variables. At an advanced stage of deformation, 'singular' elastic strain can be neglected, while a specific 'singular' variable describing intense shearing will be introduced further. We then have tentatively: $V_{regular} = \left(\mathbf{e^e}, T, p, \delta, \xi, ... \right)$ and $V_{singular} = \left(T*, p*, \delta*, \xi*, ... \right)$

Due to localization phenomena involved during the process of adiabatic shear banding, the 'singular' variables measured in any RVE located inside the band reach values which become progressively much greater than those of the 'regular' variables measured in any RVE located outside the band.

Instead of a description considering a 'small' representative volume element (RVE), i.e. whose length scale is lower than the bandwidth ($\ell < \lambda$), the more global insight is preferred

Adiabatic Shear: Pre- and Post-critical Dynamic Plasticity Modelling
and Study of Impact Penetration. Heat Generation in this Context

239

here with a 'large' RVE, i.e. whose length scale is greater than the bandwidth ($\ell > \lambda$). In this aim in view, all the set of 'singular' variables (and respective dissipation effects), and notably the 'singular' temperature T*, are incorporated in the complementary (internal) variable d whose more general definition constitutes the subject of the following.

Such a phenomenological approach must account for physical features concerning in particular ASB formation and development and the consequences of the presence of bands at the RVE scale ($\ell > \lambda$) in terms of mechanical softening, structural anisotropy and additional kinematics.

In the present approach, the evolution of the 'singular' dissipative processes contributing to the macromechanical softening is described via the evolution of an internal variable called d^{α}, α designating a family of bands with the same orientation. The softening of the global RVE behaviour being considered as a form of mechanical degradation, the variable d^{α} characterises the global material deterioration under adiabatic shear banding. It is then a function of the 'singular' state variables and of the characteristic length λ^{α} of the band:

$$d^{\alpha} = d^{\alpha}\left(\lambda, V_{singular}\right) = d^{\alpha}\left(\lambda, T*, p*, \delta*, \xi*, ...\right) \qquad (6)$$

An increase in the 'singular' temperature T* (the temperature inside the band) generates consequently increase in the magnitude of d^{α} without causing explicit increase of the 'regular' temperature T (the temperature outside the band), preserving the hypothesis of local adiabaticity.

In the same way, the structural anisotropy induced in the RVE ($\ell > \lambda$) by the presence of the bands is linked to the orientation $\mathbf{n}^{\alpha}$ of the band, through the orientation tensor $\mathbf{N}^{\alpha} = \mathbf{n}^{\alpha} \otimes \mathbf{n}^{\alpha}$.

The combination of d^{α} and $\mathbf{n}^{\alpha}$ allows for describing entirely the specific orthotropic mechanical degradation of the RVE under adiabatic shear banding. This combination is performed here through the definition of a 2nd order tensorial variable already introduced by (1), with the density d conveying singular deterioration mechanism as follows:

$$\mathbf{D} = \sum_{\alpha} d^{\alpha} . \mathbf{N}^{\alpha} ; d^{\alpha} = d^{\alpha}\left(\lambda, V_{singular}\right) = d^{\alpha}\left(\lambda, T*, p*, \delta*, \xi*, ...\right) ; \mathbf{N}^{\alpha} = \mathbf{n}^{\alpha} \otimes \mathbf{n}^{\alpha} \qquad (7)$$

As already pointed in Sect.2.1, see Eq.(2), the current density d of the deterioration tensor $\mathbf{D}$ depends notably on the 'singular' temperature T*, i.e. d=d(T*,...), the dots signifying other arguments in (7)$_2$, see also Longère et al. (2003). As $\mathbf{D}$ quantifies adiabatic shear band-induced degradation of the RVE, this variable can be considered as a sort of 'deterioration' (or damage-like) variable.

In parallel, while $\mathbf{D}$ governs the anisotropic degradation, the kinematic consequence of the presence of the band, viewed as an idealized 'super-dislocation' within the representative volume, see Fig.2 and the comments above, is dealt with by incorporating the contribution (3) to the total inelastic velocity gradient $\mathbf{L}^{dp}$ such as

$$\mathbf{L}^{dp} = \mathbf{L}^{p} + \mathbf{L}^{d} \qquad (8)$$

There are thus two contributions to the inelastic velocity gradient $\mathbf{L}^{dp}$: $\mathbf{L}^{p}$ relative to homogeneous 'regular' viscoplasticity, and $\mathbf{L}^{d}$, as mentioned above, resulting from adiabatic shear banding-induced 'singular' mechanism. The corresponding decomposition of the symmetric part of $\mathbf{L}^{dp}$, namely that of $\mathbf{d}^{dp}$, the inelastic strain rate, is given by (5) above.

2.3 Constitutive relations. Indicator for ASB-incipience

The actual modelling aims at describing the material behaviour not only during the first stage of locally homogeneous and weakly inhomogeneous deformation (stages 1 and 2 of Marchand & Duffy's curve, see Figs.1,3) but also during the phase of strong localization induced by the formation of ASB (stage 3 of Marchand & Duffy's curve, see Figs.1,3). The model should thus be robust enough to overcome local instabilities relative to inception and growth of ASB on mesoscale level.

Due to its specific scale background summarized above (Sect.2.2) by the inequality $\ell > \lambda$ and introduced in more detail in Longere et al. 2005 (Sect.1 of this reference), the model conveys implicitly a characteristic material length scale in its constitutive formulation. This implicit incorporation of the length scale becomes explicit when dealing with finite element (FE) implementation of the model and its application for structural analysis including ASB phenomena. The spatial FE discretization violating the foregoing scale level postulate is excluded. Some comments regarding this aspect and related mesh sensitivity problem are given later in Sect.3. In conclusion, the constitutive model detailed below remains apparently a local one while enfolding a scale postulate in its substructure; this represents a sort of compromise with respect to non-locality, clearly put forward in the present context by Abu Al-Rub & Voyiadjis (2006).

Based on irreversible thermodynamics with internal variables (see Coleman & Gurtin (1967), Meixner (1969) and Bataille & Kestin (1975)), the constitutive model, called TEVPD model for convenience (for 'thermoelastic/viscoplastic-deterioration'), is detailed below to be applied later in the context of high-velocity impact and penetration mechanics. Some simplifying assumptions, regarding notably strain and strain rate hardening description and small elastic strain, are made.

Kinematical considerations. The decomposition of the deformation gradient **F** as the product $\mathbf{F} = \mathbf{V}^e \mathbf{Q} \mathbf{F}^{dp}$ (see Fig.4), where $\mathbf{V}^e$ denotes the pure 'elastic' stretching ($\mathbf{F}^e = \mathbf{V}^e \mathbf{R}^e$, $\mathbf{R}^e$ the orthogonal 'elastic' rotation tensor), **Q** the rotation of anisotropy axes and $\mathbf{F}^{dp}$ the 'deterioration-plastic' i.e. inelastic deformation, allows further for following Eulerian kinematic decompositions:

$$d_{ij} = d_{ij}^e + d_{ij}^{dp} \quad ; \quad \omega_{ij} = W_{ij} + \omega_{ij}^e + \omega_{ij}^{dp} \tag{9}$$

where **d** is the total rate of strain tensor and **ω** the spin tensor. The symbols $\mathbf{d}^e$ and $\mathbf{\omega}^e$ represent respectively the elastic rate of strain and spin, $\mathbf{W} = \dot{\mathbf{Q}} \mathbf{Q}^T$ the rotation rate of anisotropy axes and $\mathbf{d}^{dp}$ and $\mathbf{\omega}^{dp}$ respectively the inelastic rate of strain and spin. The inelastic terms include regular contributions and those due to ASB evolution, namely $\mathbf{d}^d$ and $\mathbf{\omega}^d$ introduced in (4). The objective corotational derivative $\overset{\triangledown}{\mathbf{A}}$ of a 2nd order tensor **A** is given by (see e.g. Sidoroff & Dogui, 2001):

$$\overset{\triangledown}{A}_{ij} = \dot{A}_{ij} - W_{ik} A_{kj} + A_{ip} W_{pj} \tag{10}$$

Assuming small elastic deformation and a weak contribution of the plastic ('regular') spin $\mathbf{\omega}^p$ with regard to the ASB-deterioration induced spin $\mathbf{\omega}^d$ (see Longere et al., 2003, for detailed argument) the rotation rate **W** is simplified as follows:

$$W_{ij} = \omega_{ij} - \omega_{ij}^d \tag{11}$$

Adiabatic Shear: Pre- and Post-critical Dynamic Plasticity Modelling
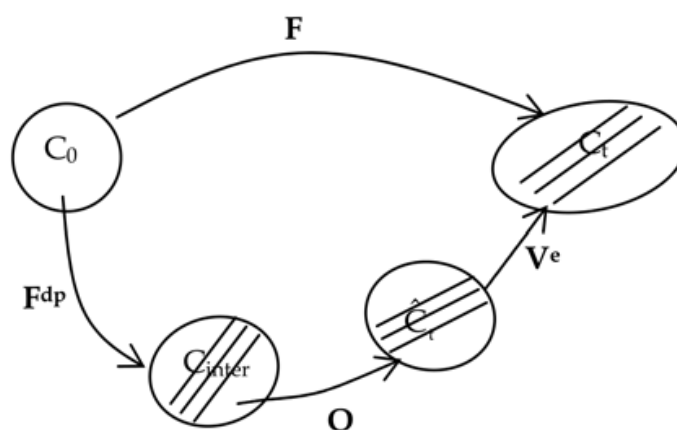and Study of Impact Penetration. Heat Generation in this Context

241

Fig. 4. Intermediate configuration and decomposition of the deformation gradient $\mathbf{F}$ in the presence of anisotropy; see also (Sidoroff & Dogui (2001))

Free energy and thermodynamic forces. In the model presented, involving 'large' RVE reference scale $\ell > \lambda$, the set of state variables referred to the actual configuration C_t is reduced to

$$V = \left(\mathbf{e}^e, T, p; \tilde{\mathbf{D}} \right)$$

with $\tilde{\mathbf{D}}$ representing a measure of the material deterioration in the current configuration due to 'singular' ASB related evolution. The tensor $\mathbf{D}$, defined in the intermediate configuration, is 'transported' to the current one, the symbol $\tilde{\mathbf{D}}$ designating the tensor $\mathbf{D}$ transformed in this way, namely $\tilde{\mathbf{D}} = \mathbf{Q}\mathbf{D}\mathbf{Q}^T$.

The set $\left(\mathbf{e}^e, T, p \right)$ corresponds exactly to the set of 'regular' state variables mentioned above while $\tilde{\mathbf{D}}$ embraces the 'singular' effects at the actual 'large' RVE scale. The tensor $\mathbf{e}^e$ represents here a spatial elastic strain measure, namely $\mathbf{e}^e = \ln(\mathbf{V}^e)$. As mentioned above, for the class of materials considered the hypothesis of small elastic strain is being assumed, i.e. ($V_{ij}^e \approx \delta_{ij} + \varepsilon_{ij}$ with $\varepsilon_{ij}\varepsilon_{ji} \ll 1$).

The thermo-elastic response of the anisotropic medium is supposed to be described by the specific free energy $\psi \left(\mathbf{e}^e, T, p; \tilde{\mathbf{D}} \right) = \psi^e \left(\mathbf{e}^e, T; \tilde{\mathbf{D}} \right) + \psi^p \left(T, p; \tilde{\mathbf{D}} \right)$ where the thermoelastic energy ψ^e and the stored energy ψ^p are assumed respectively in the form:

$$\begin{cases} \rho_0 \psi^e = \dfrac{\lambda}{2} e_{ii}^e e_{jj}^e + \mu e_{ij}^e e_{ji}^e - \alpha K e_{ii}^e \Delta T - \rho_0 c_0 \left[T \ln \left(\dfrac{T}{T_0} \right) - \vartheta \right] - a e_{kk}^e e_{ij}^e \tilde{D}_{ji} - 2 b e_{ij}^e e_{jk}^e \tilde{D}_{ki} \\ \rho_0 \psi^p = R_\infty \left[p + \dfrac{1}{k} \exp(-kp) \right] \exp(-\gamma T) \exp \left(-d_1 \tilde{D}_{ii} - \dfrac{d_2}{2} \tilde{D}_{ij} \tilde{D}_{ji} \right) \end{cases} \quad (12)$$

where λ and μ represent Lamé elasticity coefficients, K is the bulk modulus ($K = \lambda + 2\mu / 3$), α is the thermal expansion coefficient, ρ_0 the initial density, c_0 the heat capacity, $\vartheta = T - T_0$ the temperature rise, a and b the moduli related to elastic energy ASB-induced degradation and inducing a form of orthotropy. The elastic stiffness depends now on the constants λ, μ, a, b and on the actual form of $\tilde{\mathbf{D}}$. In the expression $(12)_2$ R_∞ is related to the saturation of hardening, k the plastic hardening parameter, γ the thermal softening parameter, d_1 and d_2 the deterioration (ASB) related softening constants.

The model, to be consistent with irreversible thermodynamic framework, should satisfy the Clausius-Duhem dissipation inequality. It is to be reminded that adiabatic conditions are assumed (no heat conduction). The intrinsic dissipation is expressed as follows (with respect to the current configuration):

$$D_{int} = \tau_{ij}d_{ji} - \rho_0\left(\dot{\psi} + s\dot{T}\right) \geq 0$$

with $\boldsymbol{\tau}$ designating the Kirchhoff stress tensor, s the local entropy.
The Gibbs relation and Clausius-Duhem inequality are further detailed as follows:

$$\rho_0\dot{\psi} = -\rho_0 s\dot{T} + \tau_{ij}d_{ji}^e + r\dot{p} - \tilde{k}_{ij}\overset{\triangledown}{\tilde{D}}_{ji} \;\;;\; D_{int} = \tau_{ij}d_{ji}^{dp} - r\dot{p} + \tilde{k}_{ij}\overset{\triangledown}{\tilde{D}}_{ji} \geq 0 \tag{13}$$

The thermo-elastic Kirchhoff stress tensor $\boldsymbol{\tau}$, the strain hardening thermodynamic force (affinity) r and the deterioration conjugate force $\tilde{\mathbf{k}}$ are classically derived from the thermodynamic potential $\psi\left(\mathbf{e^e}, T, p; \tilde{\mathbf{D}}\right)$ with respect to $\mathbf{e^e}$, p and $\tilde{\mathbf{D}}$:

$$\tau_{ij} = \lambda e_{kk}^e\delta_{ij} + 2\mu e_{ij}^e - \alpha K\Delta T\delta_{ij} - a\left(e_{mn}^e\tilde{D}_{nm}\delta_{ij} + e_{kk}^e\tilde{D}_{ij}\right) - 2b\left(e_{ik}^e\tilde{D}_{kj} + \tilde{D}_{ik}e_{kj}^e\right) \tag{14}$$

$$r = R_\infty\left[1 - \exp(-kp)\right]\exp(-\gamma T)\exp\left(-d_1\tilde{D}_{kk} - \frac{d_2}{2}\tilde{D}_{kl}\tilde{D}_{lk}\right) \tag{15}$$

$$\tilde{k}_{ij} = ae_{kk}^e e_{ij}^e + 2be_{ik}^e e_{kj}^e + R_\infty\left[p + \frac{1}{k}\exp(-kp)\right]\exp(-\gamma T)\exp\left(-d_1\tilde{D}_{kk} - \frac{d_2}{2}\tilde{D}_{kl}\tilde{D}_{lk}\right)\left[d_1\delta_{ij} + d_2\tilde{D}_{ij}\right] \tag{16}$$

The form of entropy $s = -\partial\psi / \partial T$ is not detailed here, see Longère et al. (2003) for this item.
Regular heating and anisotropic deterioration including singular, ASB-induced heating, contribute to reduce the stress level $\boldsymbol{\tau}\left(\mathbf{e^e}, T; \tilde{\mathbf{D}}\right)$. Constants a and b contribute both to reduce Young's modulus, while b is alone responsible for the decrease of the shear modulus.
Hardening conjugate force $r\left(T, p; \tilde{\mathbf{D}}\right)$ increases during pure hardening but decreases with heating and further deterioration effects superposed on hardening, r is thus describing the competition between plastic hardening and thermal and ASB-induced softening effects.
The ASB induced deterioration conjugate force $\tilde{\mathbf{k}}\left(\mathbf{e^e}, T, p; \tilde{\mathbf{D}}\right)$ is the energy release rate with respect to $\tilde{\mathbf{D}}$. It includes a contribution from the reversible part ψ^e of the free energy, and another one from the stored energy ψ^p. The corresponding terms represent respectively elastic and stored energy release rates induced by the formation and development of ASB in the material (RVE). It is noteworthy that both contributions to the degradation conjugate force exist before ASB inception. A finite supply of energy release rate k_{inc} is indeed assumed to be necessary to activate the deterioration process. The threshold force k_{inc} is explicitly determined by the auxiliary analysis (see Sect.2.4).
Regular vs. singular heating. The dissipation in $(13)_2$ can be decomposed into a 'regular' term directly linked to plasticity and a 'singular' term resulting from the contribution of irreversible process involving ASB:

$$D_{int} = D_{reg} + D_{sing} \;\;;\; D_{reg} = \tau_{ij}d_{ji}^p - r\dot{p} \;\;;\; D_{sing} = \tau_{ij}d_{ji}^d + \tilde{k}_{ij}\overset{\triangledown}{\tilde{D}}_{ji} \tag{17}$$

Adiabatic Shear: Pre- and Post-critical Dynamic Plasticity Modelling
and Study of Impact Penetration. Heat Generation in this Context

243

'Regular' heating $\dot{T}$ caused by plasticity outside the bands is then estimated from the relation established under the conventional adiabaticity assumption using (17)$_2$:

$$\rho_0 c_0 \dot{T} = \tau_{ij} d_{ji}^p - r\dot{p} \tag{18}$$

where c_0 represents the heat capacity.

By employing the inelastic heat fraction β, the relation (18) is reduced to:

$$\rho_0 c_0 \dot{T} = \beta \tau_{ij} d_{ji}^p \tag{19}$$

where β, depending on plastic strain, plastic strain rate and temperature (see Longère and Dragon, 2007) , is expressed by:

$$\beta = 1 - \frac{r\dot{p}}{\tau_{ij} d_{ji}^p} \tag{20}$$

The effects of 'singular' heating $\dot{T}^*$ localized inside the band cluster are included, by definition of the deterioration variable $\tilde{\mathbf{D}}$ (see (7)$_2$), in the scalar density $d(T^*,...)$, evolving with the ongoing deterioration. As a first approximation (neglecting thermomechanical coupling), one can write, using (17)$_3$:

$$\rho_0 c_0 \dot{T}^* \propto D_{sing} = \tau_{ij} d_{ji}^d + \tilde{k}_{ij} \overset{\triangledown}{\tilde{D}}_{ji} \tag{21}$$

The temperature rise effects inside the ASB are indeed included in the 'singular' dissipation which is now represented by the product $D_{sing}^D = \tilde{k}_{ij} \overset{\triangledown}{\tilde{D}}_{ji}$ in (21). The other singular term $D_{sing}^{in} = \tau_{ij} d_{ji}^d$ in (21) is due to the ASB contribution to the total inelastic strain. During the process of ASB induced degradation, the 'regular' part of dissipation decreases while the 'singular' part of dissipation increases.

Dissipation potential, yield function and evolution laws. The existence of viscous plastic and deterioration potentials of Norton-Perzyna's type is assumed in the form of a power law:

$$\phi_p^c = \frac{Y}{n+1} \left\langle \frac{F}{Y} \right\rangle^{n+1} \ ; \ \phi_d^c = \frac{Z}{m+1} \left\langle \frac{F}{Z} \right\rangle^{m+1} \tag{22}$$

where Y and n represent viscous constants relative to plasticity, Z and m viscous constants relative to (time-dependent) degradation, the bracket $\langle x \rangle = \max(x,0)$.

A single yield function F that includes both plasticity and deterioration effects appears actually suitable to describe, via the generalized normality hypothesis, the evolution of corresponding variables:

$$F\left(\tau_{ij}, r, \tilde{k}_{ij}\right) = \hat{J}_2^s\left(\tau_{ij}, \tilde{k}_{ij}\right) - \left(R_0 + r\right) ; \ \hat{J}_2^s\left(\tau_{ij}, \tilde{k}_{ij}\right) = \sqrt{\frac{3}{2} s_{ij} P_{ijkl}\left(\tilde{k}_{mn}\right) s_{kl}} \tag{23}$$

where **s** represents the deviatoric part of the Kirchhoff stress tensor, and $\mathbf{P}(\tilde{\mathbf{k}})$ the 4th order tensor inducing deterioration-prompted anisotropy of the plastic flow, assumed in the following form:

$$P_{ijkl} = \frac{1}{2}\left(\delta_{ik}\delta_{jl} + \delta_{il}\delta_{jk}\right) + 2\sum_{q=2}^{N}\eta_q\left(\tilde{k}_{mn}^{+}\tilde{N}_{nm}\right)^{q}\tilde{M}_{ij}\tilde{M}_{kl} \tag{24}$$

In the same way as $\tilde{\mathbf{D}}$, the symbols $\tilde{\mathbf{M}}$ and $\tilde{\mathbf{N}}$ designate respectively the tensors $\mathbf{M}$ and $\mathbf{N}$ (see $(4)_1$ and $(1)_2$) transported from the intermediate configuration to the current one.

In order to preserve the continuity of stress at the onset of ASB induced degradation, the deterioration driving force $\tilde{\mathbf{k}}$ intervenes via the expression $\text{Tr}\left(\tilde{\mathbf{k}}^{+}\mathbf{N}\right)$, the latter representing the difference between the current value $\text{Tr}\left(\tilde{\mathbf{k}}\mathbf{N}\right)$ and the corresponding one at the incipience of degradation $k_{inc} = \text{Tr}\left(\tilde{\mathbf{k}}\mathbf{N}\right)_{inc}$:

$$\tilde{k}_{ij}^{+}\tilde{N}_{ji} = \left\langle \tilde{k}_{ij}\tilde{N}_{ji} - k_{inc} \right\rangle \tag{25}$$

To determine k_{inc} an auxiliary analysis based on a perturbation method is conducted for a particular loading path. The function R_0 is expressed in a form similar to that of the hardening affinity except for the genuine hardening effect:

$$R_0 = R_{int}\exp(-\gamma T)\exp\left(-d_1\tilde{D}_{kk} - \frac{d_2}{2}\tilde{D}_{mn}\tilde{D}_{nm}\right) \tag{26}$$

where R_{int} represents an internal stress.

Applying the normality rule, evolution laws are derived from dissipation potentials:

$$d_{ij}^{dp} = d_{ij}^{p} + d_{ij}^{d} = \frac{\partial\phi_P^c}{\partial\tau_{ij}} = \Lambda^P\frac{\partial F}{\partial\tau_{ij}}\,;\,-\dot{p} = \frac{\partial\phi_P^c}{\partial r} = \Lambda^P\frac{\partial F}{\partial r}\,;\,\tilde{D}_{ij} = \frac{\partial\phi_d^c}{\partial\tilde{k}_{ij}} = \Lambda^d\frac{\partial F}{\partial\tilde{k}_{ij}} \tag{27}$$

The respective multipliers governing viscoplasticity and viscous deterioration are expressed by

$$\Lambda^P = \left\langle \frac{\partial\phi_P^c}{\partial F} \right\rangle = \left\langle \frac{F}{Y} \right\rangle^n\,;\,\Lambda^d = \left\langle \frac{\partial\phi_d^c}{\partial F} \right\rangle = \left\langle \frac{F}{Z} \right\rangle^m \tag{28}$$

The corresponding rates are detailed below:

$$\begin{cases} d_{ij}^{p} = \frac{3}{2}\Lambda^P\frac{s_{ij}}{\hat{J}_2^s} \\[2mm] d_{ij}^{d} = 3\Lambda^P\dfrac{\sum_{q=2}^{N}\eta_q\left(\tilde{k}_{mn}^{+}\tilde{N}_{nm}\right)^{q}s_{kl}\tilde{M}_{kl}}{\hat{J}_2^s}\tilde{M}_{ij} \end{cases} \quad \begin{cases} \dot{p} = \Lambda^P \\[2mm] \overset{\triangledown}{\tilde{D}}_{ij} = \frac{3}{2}\Lambda^d\dfrac{\sum_{q=2}^{N}q.\eta_q\left(\tilde{k}_{mn}^{+}\tilde{N}_{nm}\right)^{q-1}\left(s_{kl}\tilde{M}_{kl}\right)^2}{\hat{J}_2^s}\tilde{N}_{ij} \end{cases} \tag{29}$$

The deterioration induced spin $\boldsymbol{\omega}^d$ is deduced from (4) and $(29)_2$ as follows:

$$\omega_{ij}^{d} = 3\Lambda^P\dfrac{\sum_{q=2}^{N}\eta_q\left(\tilde{k}_{mn}^{+}\tilde{N}_{nm}\right)^{q}s_{kl}\tilde{M}_{kl}}{\hat{J}_2^s}\tilde{T}_{ij} \tag{30}$$

$\tilde{\mathbf{T}}$ is again (as is $\tilde{\mathbf{M}}$) the tensor $\mathbf{T}$ (see $(4)_2$) expressed in the actual configuration C_t.

Adiabatic Shear: Pre- and Post-critical Dynamic Plasticity Modelling
and Study of Impact Penetration. Heat Generation in this Context

245

The evolution laws (29) verify the collinearity of the 'regular' plastic strain rate $\mathbf{d}^p$ with the deviatoric part $\mathbf{s}$ of the Kirchhoff stress tensor, the collinearity of the 'singular' ASB-induced strain rate $\mathbf{d}^d$ with the orientation tensor $\tilde{\mathbf{M}} = \left[\tilde{\mathbf{g}} \otimes \tilde{\mathbf{n}}\right]^S$ (note that $\tilde{\mathbf{T}} = \left[\tilde{\mathbf{g}} \otimes \tilde{\mathbf{n}}\right]^{AS}$), according to (4), and finally the collinearity of the damage rate $\overset{\triangledown}{\tilde{\mathbf{D}}}$ with the orientation tensor $\tilde{\mathbf{N}} = \tilde{\mathbf{n}} \otimes \tilde{\mathbf{n}}$ for conservative damage growth configuration considered here tentatively. On the other hand, the form of the polynomial in $\text{Tr}\left(\tilde{\mathbf{k}}^+\tilde{\mathbf{N}}\right)$, starting with the exponent q=2 (see (29)$_2$ and

(29)$_4$), ensures the concomitance of the deterioration induced rates $\mathbf{d}^d$ and $\overset{\triangledown}{\tilde{\mathbf{D}}}$. The adiabatic shear banding process which generates the supplementary inelastic strain rate $\mathbf{d}^d$ modifies the initial direction of the inelastic strain rate $\mathbf{d}^p$.

Auxiliary indicator for deterioration incipience. The constitutive model summarized above is completed by a deterioration incipience criterion based on a simplified analysis of material instability using the linear perturbation method. It is not detailed here, the reader can consult the references (Molinari, 1985, Longère et al., 2003, Longère & Dragon, 2007) for this approach. The auxiliary simplified analysis performed here is intended to help to establish ASB induced degradation incipience threshold and its form based on more pertinent indications than purely phenomenological formulation (see e.g. Batra & Lear, 2005, for phenomenological proposals). The general (three-dimensional) criterion obtained is as follows:

$$G\left(\tau_{ij}, r, \dot{p}; \frac{\partial r}{\partial p}, \frac{\partial r}{\partial T}\right) = \sqrt{3}\left|\tau_{res}\right| - \left(r - \frac{1}{n}Y\dot{p}^{\frac{1}{n}} + \rho_0 c_0 \left(\frac{\partial r}{\partial p} / \left(-\frac{\partial r}{\partial T}\right)\right)\right) > 0 \qquad (31)$$

where $\tau_{res} = \text{Tr}\left(\mathbf{s}\tilde{\mathbf{M}}\right)$ represents the resolved shear stress for a loading path at stake, r the isotropic hardening conjugate force, $Y\dot{p}^{1/n}$ the strain rate-induced overstress, $\partial r / \partial p$ the plastic hardening and $\partial r / \partial T$ the thermal softening effects. In the present simplified analysis (see Longère et al. (2003) for further details), the deterioration process is actually assumed to run as soon as $G = 0$. The condition (31) must be interpreted as the auxiliary indicator for the deterioration process incipience leading to the determination of the deterioration conjugate force threshold $k_{inc} = \text{Tr}\left(\tilde{\mathbf{k}}\tilde{\mathbf{N}}\right)_{inc}$ in (25), for the stress-state $\boldsymbol{\tau}$.

3. Application: initial/boundary value problem involving dynamic shearing

3.1 Preliminaries: numerical procedure and HSS testing/simulation

This section aims at determining numerically the plugging conditions for an armour steel plate submitted to the impact of a fragment-simulating projectile (FSP). During the FSP/plate interaction, the ultimate failure of the plate is here preceded by adiabatic shear banding, as it is often the case with high strength steel plates.

Numerical procedure. The three-dimensional constitutive TEVPD model presented in Sect.2 has been implemented as 'user material' in the finite element code LS-DYNA®.

Integration of constitutive equations in the case of softening behaviour is not trivial, and there is no standard procedure. It is well-known that viscosity contributes to 'regularize' the boundary value problem but in the present case (strong localization induced by ASB formation) a complementary procedure was needed to overcome numerical locking in the context of explicit numerical scheme. The adaptive time step procedure adopted herein is

based on the principle of the maximal strain increment and consists in sampling, i.e. partitioning, the 'global' time increment (the time increment determined by the code itself for integrating the equations of motion). By reducing the 'local' time increment (the time increment used for integrating constitutives equations), for the element concerned and not for the whole structure, it ensures numerical convergence and stability as stated by Kulkarni et al. (1995). This procedure leads to an equivalence with a damage-like model with a 'controlled rate', see e.g. Suffis et al. (2003), assuring that the $\tilde{\mathbf{D}}$-rate here tends never to infinity and that there is very limited (if any) mesh sensitivity effect for a post-localization stage (for some details regarding mesh dependency analysis see Longère et al. (2005)).

Experimental procedure. Prior to carrying out the ballistic penetration simulation, it is necessary to characterize the material behaviour of both the FSP and the plate under dynamic loading. In this aim in view, the FSP and the plate materials have been tested under compressive loading using the split Hopkinson pressure bar (SHPB) device. The plate material has also been tested under simple shear loading using the split Kolsky bar device. The experimental data have been used to determine the viscoplasticity (plastic flow, strain hardening, thermal softening) and ASB-deterioration related material constants of the present model. The set of constants has been validated by confronting experimental and numerical results obtained from the dynamic shearing of a hat shape structure (HSS) composed of the plate material. These dynamic shearing tests provide furthermore a failure criterion which is used in the simulation of the ballistic penetration problem. This criterion is interpreted here tentatively in term of admissible deterioration state. The method consists practically in determining a critical value for the quantity $\text{Tr}\tilde{\mathbf{D}}$, i.e. $\text{Tr}\tilde{\mathbf{D}}_c$, for which the failure is observed experimentally. From the numerical viewpoint, as $\text{Tr}\tilde{\mathbf{D}}$ reaches the value $\text{Tr}\tilde{\mathbf{D}}_c$ in a finite element, the corresponding element is eroded, allowing for the formation/propagation of a crack.

3.2 Ballistic penetration problem. Numerical simulation

We are now examining the interaction between a fragment simulating projectile (FSP) and a semi-thick target metal plate regarding the engineering problem of ballistic penetration (see DeLuca et al. (1998) and Mahfuz et al. (2000), for applications involving FSP/composite material plate interaction). According to the relative value of the diameter (2R) of the FSP and the thickness (H) of the plate in relation to the FSP length and initial velocity, the expected failure mode of the plate is plugging (see Backman & Goldsmith (1978) and Woodward (1990) for exhaustive review of penetration induced phenomena) which is known to occur as the result of adiabatic shearing process. The penetration is indeed accompanied by the formation of annular adiabatic shear bands. In the case of a projectile harder than the plate, the progressively formed annulus of ASB and further fracture zone has a diameter equal to the initial diameter of the projectile and the failure mode is typically punching. In the case of a projectile and a semi-thick plate with a very close hardness, there is generally formation of a 'first' progressive annulus of ASB with a diameter equal to the initial diameter of the projectile followed by the formation of a 'second' progressive annulus of ASB with a diameter greater than the initial diameter of the projectile. The former, which forms early, does not cross entirely the thickness of the plate and is not responsible for the ultimate failure; the second annulus, which forms later, is due to the radial expansion of the projectile during deformation and is responsible for the ultimate failure. This process

characterizes the failure mode of plugging. This feature constitutes a major criterion that may discriminate various models and related numerical simulations of the penetration process and failure under plugging.

The discrete model used for numerical simulation via LS-DYNA computation code is shown in Fig.5. It is to be noted that no particular zone has been finely meshed because the ASB trajectory is supposed to be unknown. On the other hand, during the numerical simulation, no adaptive mesh refinement has been used.
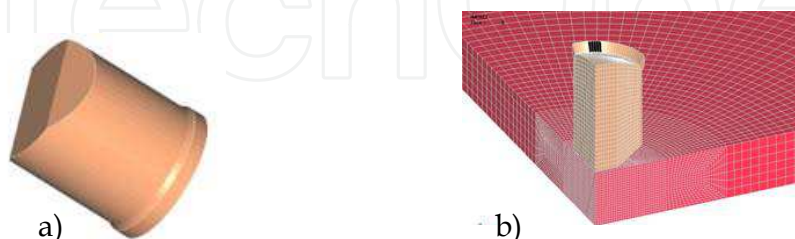

Fig. 5. Geometry and spatial discretization of the FSP and the plate; a) FSP geometry; **b)** Spatial discretization

The hard steel projectile material behaviour is modelled with Johnson and Cook law, see Johnson & Cook (1983), while the hard steel plate behaviour is described via TEVPD model, see Table 1 – the respective materials are different. An erosion criterion in term of critical cumulated plastic strain p_c has been applied to both the projectile and the plate. Concerning the plate a complementary erosion criterion in term of critical ASB-induced degradation state $\text{Tr}\tilde{\mathbf{D}}_c$ has also been applied. The former is indeed very suitable for managing the boundary erosion at the FSP/plate interface at the impact (normal contact) and during the penetration (tangential contact). The latter is used for ASB-induced internal failure.

As mentioned previously, the values of material constants relative to the TEVPD model have been determined from compression and torsion dynamic tests and failure/erosion critical value $\text{Tr}\tilde{\mathbf{D}}_c$ from HSS dynamic shearing tests. For confidentiality reason no value can be given.

$\rho_0 = 7800 \text{ kg/m}^3$	$c_0 = 420 \text{ J/kg.K}$	$E = 200 \text{ GPa}$	$\nu = 0.33$	$\alpha = 1.\text{e-}6 \text{ K}^{-1}$
$R_{int} = 920 \text{ MPa}$	$R_\infty = 400 \text{ MPa}$	$k = 10$	$\gamma = 1.1\text{e-}3 \text{ °C}^{-1}$	$Y = 60 \text{ MPa.s}^{1/n}$
$n = 6$	$a = 0$	$b = 15 \text{ GPa}$	$d_1 = 0.05$	$d_2 = 0.05$
$\eta_2 = 0.12 \text{ MPa}^{-2}$	$Z = 19 \text{ MPa.s}^{1/m}$	$m = 2$		

Table 1. Plate material constants for numerical simulation (30 NiCrMo6-6 steel)

Fig.6 shows numerical diagrams of the plate for a configuration with a FSP initial velocity V_{FSP} equal to 95 % of the ballistic limit V_{bpl} (Fig.6a) and for a configuration with a FSP initial velocity V_{FSP} equal to 105% of V_{bpl} (Fig.6b). The numerical simulation including the TEVPD model for the plate is thus able to reproduce the plugging of the plate near the ballistic limit. We are now analysing the process which leads to failure. According to Fig.6 the projectile is subject to large deformation due to very close hardness of the plate and itself. Fig.6a shows two families of deteriorated FE bands: the early ones which are concentrated in an annulus with a diameter close to the initial diameter of the projectile and the late bands which are

concentrated in an annulus with a diameter greater than the initial diameter of the projectile. The failure (erosion) following ASB-induced deterioration within the late bands occurs first inside the plate and propagates to the surface forming a macro-crack which leads for a higher velocity to plugging (see Fig.6b) – Mode II like crack propagation.
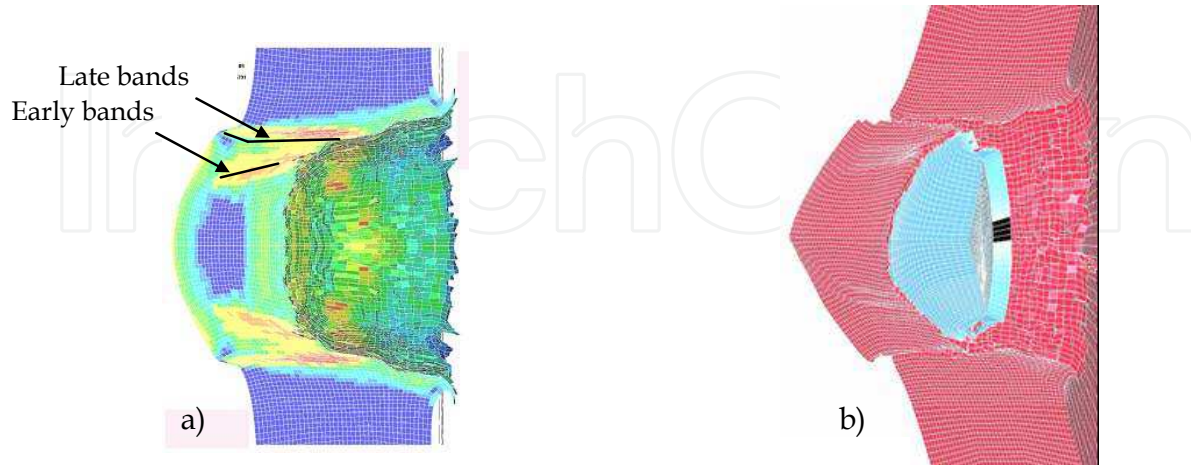

Fig. 6. Numerical views of the deformed plate ($\mathrm{Tr}\tilde{\mathbf{D}}$) for FSP initial velocity V_{FSP} lower a) and higher b) than the ballistic penetration limit velocity V_{bpl} (H=2R)

In order to evaluate the predictive ability of the model, a series of numerical tests of influence has been carried out. They concern first the influence of some TEVPD model constants, then the influence of the model for the plate, and finally the influence of the mesh size.

Influence of TEVPD model constant k. The first comparative study is devoted to the influence of the isotropic plastic hardening modulus k which appears explicitly in the expression of the isotropic hardening conjugate force r (15) and also in the deterioration incipience criterion (31) via r and its partial derivatives. In the sense that it describes the material hardening kinetics– the greater is k the faster the saturation stress is reached – the instability (and further localization) is anticipated or delayed depending on the magnitude of k. Some numerical simulations have shown that increasing k leads to decreasing of the shear strain at localization onset in the case of dynamic simple shear and to accelerating formation of crossing bands in the case of dynamic shearing of HSS.

According to Fig.7a, showing the deterioration map in the configuration with a low value of k, three families of bands appear. The family 1 is formed early, the family 2 after it and the family 3 ultimately. The family 1 has crossed the plate thickness and provokes a striction at the plate rear. The deformation localizes then in the striction zone while the other families of bands slacken their progression. In the configuration with a higher value for k (see Fig.7b), the families 1 and 2 are group together without crossing the plate thickness while the family 3 propagation is complete and yields to a striction at the plate rear. These two configurations show two types of localized deformation processes depending on the plate material and particularly its hardening ability. This statement shows that the boundary value problem involves both structural and material effects, the latter being less significant in the case of thin plates.

Influence of the model for the plate material. Engineering problems of ballistic penetration are often carried out employing the Johnson and Cook law, see Johnson & Cook (1983), as constitutive model. This application-oriented model describes the combined effects of strain hardening, thermal softening and plastic viscosity, but does not incorporate any anisotropic
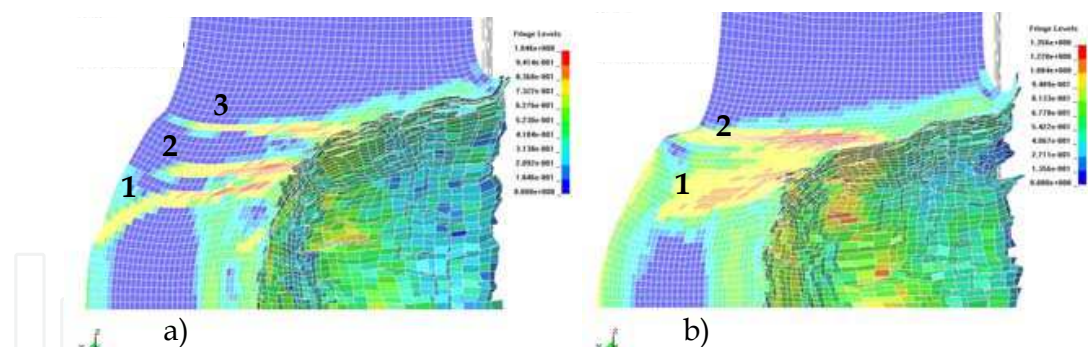
Adiabatic Shear: Pre- and Post-critical Dynamic Plasticity Modelling
and Study of Impact Penetration. Heat Generation in this Context

249

Fig. 7. Influence of the value of the constant k (hardening) of the TEVPD model. Numerical deterioration ($\text{Tr}\tilde{\mathbf{D}}$) map in the configuration with H=2R at the same time for a FSP initial velocity lower than the ballistic limit; a) k=10; b) k=30

deterioration under adiabatic shear banding. To palliate this deficiency in simulation involving the mechanism of localized deformation, the use of Johnson and Cook model necessitates meshing initially very finely the zone in which the band is supposed to propagate, the mesh size being lower than the bandwidth (see e.g. Børvik et al., 2001). This method implies the *a priori* knowledge of the band trajectory because usually it is not envisioned to mesh finely the whole structure. It may lead to favour the deformation localization in the finely meshed zone to the detriment of other potential propagation areas. An alternative method consists in using an adaptive mesh refinement technique (see e.g. Camacho & Ortiz, 1997) which remains nevertheless still costly in term of computation. Supposing this limitation overcome, the phenomenon of adiabatic shear banding generates in the concerned finite elements very high strain rates (10^5-10^6 s^{-1}), in any way much greater than the strain rates involved in the mechanical tests for the model constants identification. In this sense the material behaviour in the ASB affected FE is *de facto* uncorrectly described.

In the methodology proposed in this paper the finite element must contain the band, remind the scale postulate $\ell > \lambda$ put forward in Sect.2 and commented further. In other words, the bandwidth must be lower than the mesh size. Satisfying this condition, a simulation with Johnson and Cook law and a simulation with the TEVPD model for the metal plate have been performed. Corresponding numerical results for a FSP initial velocity lower than the ballistic limit are shown in Fig.8. According to Fig.8a, the simulation with Johnson and Cook model does not show any localization area at the time considered. On the contrary the simulation with the TEVPD model, Fig.8b, reveals at the same time a band of localized deformation which propagates through the thickness of the plate and produces some striction at the plate rear. This is clearly the consequence of the incorporation of ASB induced deterioration together with the specific scale postulate in the TEVPD model.

Influence of the mesh size. The last part of this section deals with the influence of the mesh size which is the restrictive point for numerical simulations in the presence of localization phenomena. One should insist here once more on the scale postulate put forward as the TEVPD modelling premise. Its consequence is that the band must be embedded in the finite element. This point, regarding standard simulation requiring dense meshing (at least locally), does not mean that any mesh size is suitable. The scale postulate comes to be fairly satisfied in practice for a mesh size about 5 times the material bandwidth, i.e. for a steel considered here, for about 500 μm and more. This is the case for the configuration in Fig.9a. The configuration in Fig.9b for a coarse meshing shows an expanded area of deteriorated

finite elements. This discrepancy is also induced by a rough treatment of the contact FSP/plate interaction and not only by localization effects.
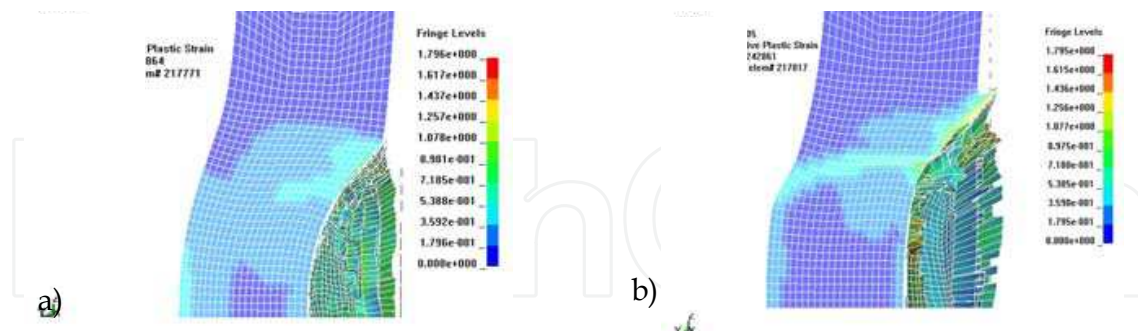

Fig. 8. Plastic deformation (p) map in the configuration with H=R at the same time for a FSP initial velocity lower than the ballistic limit; a) Johnson-Cook model; b) TEVPD model
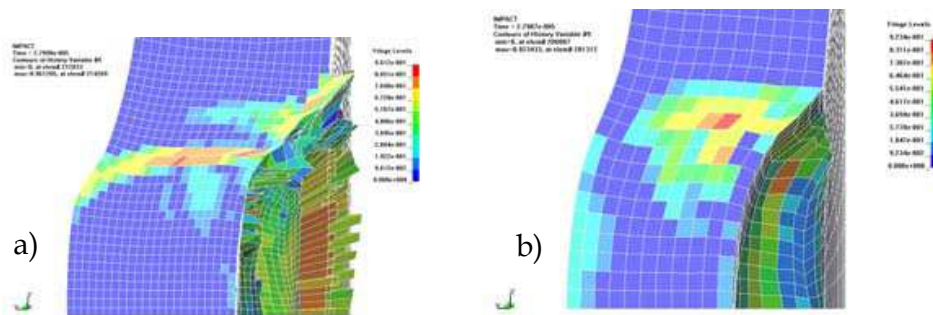

Fig. 9. Numerical deterioration ($\mathrm{Tr}\tilde{\mathbf{D}}$) map in the configuration with H=R at the same time for a FSP initial velocity lower than the ballistic limit; a) a=0.5mm; b) a=1mm

4. Evaluation of the inelastic heat fraction in the context of microstructure-supported dynamic plasticity modelling

4.1 Basic concepts and unified approach

Under dynamic adiabatic conditions the plastic work is known to dissipate into heat and inducing thermal softening. From both theoretical and numerical viewpoints the proportion of effectively dissipated plastic work is commonly evaluated using the so-called Taylor-Quinney coefficient (Taylor & Quinney, 1934) usually assumed to be a constant empirical value. On the other hand experimental investigations have shown its dependence on strain, strain rate and temperature.

A methodology combining dislocation theory in the domain of thermally activated inelastic deformation mechanisms and internal variable approach applied to thermo-elastic/viscoplastic behaviour is developed allowing for obtaining a physically based inelastic heat fraction expression. The latter involves explicitly the combined influence of the parameters mentioned above and highly evolving nature of the inelastic heat fraction.

This section aims at reconciling two main methodologies of modelling, namely the physically based, i.e. dislocation kinetics related formalism and the phenomenological one. In a first sub section the former is briefly applied to plastic deformation mechanisms controlled by thermal activation in the cases of fcc and bcc materials. Afterwards the irreversible thermodynamics related internal variable procedure is considered regarding

Adiabatic Shear: Pre- and Post-critical Dynamic Plasticity Modelling
and Study of Impact Penetration. Heat Generation in this Context

251

thermo-elastic/viscoplastic materials. In the last sub section a unified approach is employed in which the dislocation interaction mechanisms based modelling is incorporated in the formalism of standard generalized materials.

Dislocation mechanics based modelling. The following modelling is devoted to metallic materials which deform plastically under dislocation motion and accumulation/ annihilation mechanisms. It refers explicitly to the concept of thermally controlled mechanisms. In the range of strain rate (high enough to consider the deformation mechanisms as thermally activated but low enough to exclude the phonon drag phenomenon) and temperature considered, the resistance to dislocation motion is supposed to be due to two kinds of obstacles: long-range barriers typically formed by grain boundaries and other far-field influent microstructural elements relative to a rate and temperature independent stress (athermal stress), and short-range barriers formed by disoriented dislocations and other point defects relative to a rate and temperature dependent stress (thermal/viscous stress). According to this framework, the flow stress τ may be decomposed into an athermal contribution τ_a and a thermal/viscous contribution τ_{th} as follows:

$$\tau = \tau_a\left(\gamma^p\right) + \tau_{th}\left(\gamma^p, \dot{\gamma}^p, T\right) \tag{32}$$

where γ^p represents the plastic strain, $\dot{\gamma}^p$ the plastic strain rate and T absolute temperature. The athermal stress τ_a reflects the influence of the presence of solute, original dislocation density and grain size (the material state considered here is not the virgin one if the material was submitted to thermo-mechanical treatments) through a constant contribution τ_0 and the accumulation of dislocation through a hardening contribution $\overline{\tau}$. Assuming a bounded dislocation density at large deformation, the hardening stress is supposed to saturate, following Voce's form:

$$\tau_a\left(\gamma^p\right) = \tau_0 + \overline{\tau}\left(\gamma^p\right); \quad \overline{\tau}\left(\gamma^p\right) = \tau_\infty\left[1 - \exp\left(-b\gamma^p\right)\right] \tag{33}$$

where τ_∞ represents the maximum hardening stress and b a material constant characterizing the hardening kinetics.

According to Orowan's law in the context of thermally activated inelastic mechanisms, the plastic strain is assumed in the following Arrhenius form, where the constant pre-exponential term $\dot{\gamma}_0$ is notably related to mobile dislocation density and obstacle overcoming frequency, k represents the Boltzmann constant and ΔG the activation energy or energetic barrier needed for dislocation to overcome:

$$\dot{\gamma}^p = \dot{\gamma}_0 \exp\left(-\frac{\Delta G}{kT}\right) \; ; \; \Delta G = G_0\left[1 - \left\langle\frac{\tau_{th}}{\hat{\tau}}\right\rangle^w\right]^q \tag{34}$$

where the total energy G_0 is related to the material strain-rate sensitivity via the activation volume, $\hat{\tau}$ the maximum glide resistance, and w and q express the statistical shape of the obstacle profile. According to (34), one obtains

$$\dot{\gamma}^p = \dot{\gamma}_0 \exp\left\{-\frac{G_0}{kT}\left[1 - \left\langle\frac{\tau_{th}}{\hat{\tau}}\right\rangle^w\right]^q\right\} \; ; \; \tau_{th} = \hat{\tau}\left\{1 - \left[-\frac{kT}{G_0}\ln\left\langle\frac{\dot{\gamma}^p}{\dot{\gamma}_0}\right\rangle\right]^{1/q}\right\}^{1/w} \tag{35}$$

In the case of bcc materials, the maximum glide resistance $\hat{\tau}$ is assumed to be a constant, i.e. $\hat{\tau} = \hat{\tau}_0$, yielding the following form for the total flow stress:

$$\tau = \tau_0 + \tau_\infty \left[1 - \exp\left(-b\gamma^p\right) \right] + \hat{\tau}_0 \left\{ 1 - \left[-\frac{kT}{G_0} \ln \left\langle \frac{\dot{\gamma}^p}{\dot{\gamma}_0} \right\rangle \right]^{1/q} \right\}^{1/w} \tag{36}$$

This expression for the bcc material flow stress reflects experimental observations showing that, for isothermal processes, the apparent strain hardening $d\tau / d\gamma^p$ is neither affected by strain rate at a given initial temperature nor by initial temperature at a given strain rate. This explains the additive decomposition of the flow stress into separated strain hardening contribution and thermal/viscous contribution (see Zerilli & Armstrong, 1987, and Voyiadjis & Abed, 2006).

In the case of fcc materials, the maximum glide resistance is assumed to involve the former athermal stress contribution affected by temperature. Let us consider the following expression corresponding to a simplification of other more complex forms available in literature (see, e.g. Nemat-Nasser & Li, 1998):

$$\hat{\tau} = \left[\tau_0 + \bar{\tau}(\gamma) \right] a(T) \; ; \; a(T) = 1 - \left(\frac{T}{T_m} \right)^2 \tag{37}$$

According to (32), (33), (35)$_2$ and (37) the total flow stress for fcc material is thus given by

$$\tau = \left\{ \tau_0 + \tau_\infty \left[1 - \exp\left(-b\gamma^p\right) \right] \right\} \left[1 + \left[1 - \left(\frac{T}{T_m} \right)^2 \right] \left\{ 1 - \left[-\frac{kT}{G_0} \ln \left\langle \frac{\dot{\gamma}^p}{\dot{\gamma}_0} \right\rangle \right]^{1/q} \right\}^{1/w} \right] \tag{38}$$

Contrarily to bcc materials, the flow stress for fcc materials is known to combine multiplicatively the influence of both strain hardening and thermal/viscous contributions (see Zerilli & Armstrong, 1987, and Voyiadjis & Abed, 2005). This feature is respected in expression (38).

Thermodynamic framework. Following irreversible thermodynamics framework detailed in Sect.2.3, the instantaneous state of the material is supposed to be described via the free energy $\tilde{\psi} = \rho\psi$, with $\tilde{\psi}\left(T; \mathbf{e}^e, p\right)$, such that

$$\dot{\tilde{\psi}} = \frac{\partial\tilde{\psi}}{\partial T}\dot{T} + \frac{\partial\tilde{\psi}}{\partial\mathbf{e}^e} : \mathbf{d}^e + \frac{\partial\tilde{\psi}}{\partial p}\dot{p} = -\tilde{s}\dot{T} + \boldsymbol{\sigma} : \mathbf{d}^e + r\dot{p} \; ; \; \tilde{s} = -\frac{\partial\tilde{\psi}}{\partial T} \; ; \; \boldsymbol{\sigma} = \frac{\partial\tilde{\psi}}{\partial\mathbf{e}^e} \; ; \; r = \frac{\partial\tilde{\psi}}{\partial p} \tag{39}$$

where $\mathbf{d}^e = \overset{\triangledown}{\mathbf{e}^e} = \dot{\mathbf{e}}^e - \boldsymbol{\omega}\mathbf{e}^e + \mathbf{e}^e\boldsymbol{\omega}$, $\triangledown$ representing the objective Jaumann derivative of a 2nd order tensor and $\boldsymbol{\omega} = \left[\mathbf{L}\right]^{AS}$ the spin. According to the second principle of thermodynamics intrinsic mechanical dissipation is written as

$$D_{int} = \boldsymbol{\sigma} : \mathbf{d}^p - r\dot{p} \geq 0 \tag{40}$$

where $\boldsymbol{\sigma} : \mathbf{d}^p$ represents the plastic part of the mechanical work rate and $r\dot{p}$ the stored energy rate. Combining (39) with the first law of thermodynamics and assuming that r is

Adiabatic Shear: Pre- and Post-critical Dynamic Plasticity Modelling
and Study of Impact Penetration. Heat Generation in this Context

253

independent of temperature (see $(44)_2$ below) lead to the following form for the heat equation:

$$\tilde{c}_y \dot{T} + \mathrm{div}\mathbf{Q} - R = T\frac{\partial \boldsymbol{\sigma}}{\partial T} : \mathbf{d^e} + \boldsymbol{\sigma} : \mathbf{d^p} - r\dot{p} \tag{41}$$

where $\tilde{c}_y$ $\left(\tilde{c}_y = -T\partial^2\tilde{\psi}/\partial T^2\right)$ represents the heat capacity per unit mass at fixed y, $y = \left(\mathbf{e^e},p\right)$, $\mathbf{Q}$ heat flux vector per unit surface and R heat supply per unit volume. The context considered herein concerns loading at high strain rate excluding heat supply and for which conditions can be assumed as adiabatic. Relation (41) above is thus reduced to

$$\tilde{c}_y \dot{T} = T\frac{\partial \boldsymbol{\sigma}}{\partial T} : \mathbf{d^e} + \boldsymbol{\sigma} : \mathbf{d^p} - r\dot{p} = D_{int} + T\frac{\partial \boldsymbol{\sigma}}{\partial T} : \mathbf{d^e} \tag{42}$$

where $T\left(\partial \boldsymbol{\sigma}/\partial T\right) : \mathbf{d^e}$ represents the thermo-elastic coupling contribution. Considering that $D_{int} \geq 0$ and $T\left(\partial \boldsymbol{\sigma}/\partial T\right) : \mathbf{d^e} \leq 0$ for tensile loading (implying cooling) or $T\left(\partial \boldsymbol{\sigma}/\partial T\right) : \mathbf{d^e} \geq 0$ for compressive loading (implying heating), thermo-elastic and thermo-viscoplastic mechanisms act in an opposite or like way regarding temperature rise.

According to the aforementioned assumptions, the free energy $\tilde{\psi}\left(T;\mathbf{e^e},p\right)$ is now expressed in the following form:

$$\tilde{\psi}\left(T;\mathbf{e^e},p\right) = \frac{\lambda}{2}\left(\mathrm{Tr}\mathbf{e^e}\right)^2 + \mu\mathbf{e^e} : \mathbf{e^e} - \alpha K\mathrm{Tr}\mathbf{e^e}\vartheta - \tilde{c}_0\left[T\ln\left(\frac{T}{T_0}\right) - \vartheta\right] + h(p) - h(0) \tag{43}$$

where the heat capacity $\tilde{c}_y$ is supposed to have a constant value, i.e. $\tilde{c}_y = \tilde{c}_0$, and where $h(p)$ represents the stored energy of cold work as a function of strain hardening variable. After partial derivation of (43) with respect to state variables, the thermodynamic forces are

$$\boldsymbol{\sigma} = \left(\lambda\mathrm{Tr}\mathbf{e^e} - \alpha K\vartheta\right)\boldsymbol{\delta} + 2\mu\mathbf{e^e} \; ; \; r = h'(p); \; \tilde{s} = \alpha K\mathrm{Tr}\mathbf{e^e} + \tilde{c}_0\ln\left(T/T_0\right) \tag{44}$$

The dissipation potential is assumed of the Perzyna's type, i.e. $\phi(\boldsymbol{\sigma},r) = \phi\left(\langle F(\boldsymbol{\sigma},r)\rangle\right)$. The viscoplastic multiplier Λ^P and the yield function F are assumed as

$$\Lambda^P = \frac{\partial\phi}{\partial F} = H\left(\langle F(\boldsymbol{\sigma},r)\rangle\right) \geq 0 \; ; \; F(\boldsymbol{\sigma},r) = J_2(\boldsymbol{\sigma}) - g(r) \; ; \; J_2(\boldsymbol{\sigma}) = \sqrt{\frac{3}{2}\mathbf{s} : \mathbf{s}} \; ; \; \mathbf{s} = \boldsymbol{\sigma} - \frac{\mathrm{Tr}\boldsymbol{\sigma}}{3}\boldsymbol{\delta} \tag{45}$$

where H is a function of the yield surface F. The strain hardening function g(r) in (45) represents the von Mises surface radius. It is assumed in the form

$$g(r) = R_0 + r(p) \tag{46}$$

It includes the first term R_0 independent of strain hardening and the isotropic hardening force r as the second term. The quantity R_0 accounts for residual stresses potentially induced by the previous thermo-mechanical history of the material. Assuming normality rule, evolution laws are expressed by

$$\mathbf{d^p} = \frac{3}{2}\Lambda^P\frac{\mathbf{s}}{J_2(\boldsymbol{\sigma})} \; ; \; \dot{p} = \Lambda^P \tag{47}$$

Inverting $(45)_1$ and using $(45)_2$ and (46) yield

$$J_2 = R_0 + r(p) + \Phi(p, \dot{p}, T) \; ; \; \Phi = H^{-1} \tag{48}$$

The rate of plastic work $\boldsymbol{\sigma} : \mathbf{d}^p$ and the dissipation in (40) are thus given by

$$\boldsymbol{\sigma} : \mathbf{d}^p = J_2 \dot{p} = \left[R_0 + r(p) + \Phi(p, \dot{p}, T) \right] \dot{p} \; ; \; D_{int} = \left[R_0 + \Phi \right] \dot{p} \geq 0 \tag{49}$$

Dislocation mechanics-irreversible thermodynamics unified approach. The concepts of thermally activated processes developed previously are now incorporated in the internal variable procedure formalism (see also Voyiadjis & Abed, 2006). The first step consists in unifying the notations. The corresponding terms are reported in Table 2. The following yield function describing athermal processes is also assumed (see Eqs. (32)(33) and $(45)_2(46)$):

$$F(\tau, \overline{\tau}) = \tau - (\tau_0 + \overline{\tau}) = F(\boldsymbol{\sigma}, R) = J_2(\boldsymbol{\sigma}) - (R_0 + r) \tag{50}$$

Noting that $\tau_{th}(\gamma, \dot{\gamma}, T) = \tau - \tau_a(\gamma) = F(\tau, \overline{\tau}) \geq 0$ stands for viscoplastic yielding, expression $(35)_1$ is converted into

$$\dot{p} = \dot{p}_0 \exp \left\{ -\frac{G_0}{kT} \left[1 - \left\langle \frac{F(\boldsymbol{\sigma}, R)}{\hat{\tau}} \right\rangle^w \right]^q \right\} = H \langle F(\boldsymbol{\sigma}, R) \rangle \tag{51}$$

Expression (48) has to be compared to the following one obtained from Eqs. (32) and (33):

$$\tau = \tau_0 + \overline{\tau}(\gamma^p) + \tau_{th}(\gamma^p, \dot{\gamma}^p, T) \tag{52}$$

Dislocation mechanics	Internal variable procedure
γ^p	p
$\dot{\gamma}^p$	$\dot{p}$
τ	J_2
$\tau_a(\gamma^p) = \tau_0 + \overline{\tau}(\gamma^p)$	$g(p) = R_0 + r(p)$
τ_0	R_0
$\overline{\tau}(\gamma^p) = \tau_\infty \left[1 - \exp(-b\gamma^p) \right]$	$r(p) = R_\infty \left[1 - \exp(-bp) \right]$
$\tau_{th}(\gamma, \dot{\gamma}, T)$	$\Phi(p, \dot{p}, T)$
τ_∞	R_∞

Table 2. Corresponding terms for dislocation mechanics-irreversible thermodynamics unified approach

4.2 Application for fcc and bcc materials: evolving character of the inelastic heat fraction

According to the dislocation mechanics-irreversible thermodynamics unified viscoplasticity approach developed previously, this section aims at showing the influence of the modelling regarding the evolution of the inelastic heat fraction and related temperature rise. Actually it is shown that, from the thermodynamic viewpoint, the inelastic heat fraction rate is strongly

Adiabatic Shear: Pre- and Post-critical Dynamic Plasticity Modelling
and Study of Impact Penetration. Heat Generation in this Context

255

dependent on the strain hardening/softening rate. Fcc and bcc materials are modelled and the inelastic heat fraction is deduced in both cases. Its evolution is analysed considering a simple shear loading.

General expression for the inelastic heat fraction. In the following the effects of strain hardening, thermal softening and viscosity on stress/strain behaviour, temperature rise and inelastic heat fraction are studied. Thermo-elastic coupling contribution to temperature rise is actually particularly significant in problems involving very high velocity impact and/or high pressure shock loading. In the context of this work, velocity and pressure are considered moderately high and thermo-elastic coupling is neglected. Heat equation in (42) is thus reduced to

$$\tilde{c}_0 \dot{T} = D_{int} \tag{53}$$

Starting from the definition of the inelastic heat fraction β as $\beta = \tilde{c}_0 \dot{T} / \boldsymbol{\sigma} : \mathbf{d^p}$, the following expression is deduced:

$$\beta = 1 - \frac{r\dot{p}}{\boldsymbol{\sigma} : \mathbf{d^p}} \tag{54}$$

Accounting for Eq. (49)$_1$, relations (53) and (54) become

$$\dot{T} = \frac{1}{\tilde{c}_0}[J_2 - r]\dot{p} = \frac{R_0 + \Phi(p,\dot{p},T)}{\tilde{c}_0}\dot{p} \quad ; \quad \beta = 1 - \frac{r}{J_2} = 1 - \frac{h'(p)}{R_0 + h'(p) + \Phi(p,\dot{p},T)} \tag{55}$$

Consequently, the inelastic heat fraction β appears explicitly as a function of thermal/athermal hardening/softening and viscosity mechanisms via $\Phi(p,\dot{p},T)$ and $h'(p)$ and of the prior plastic deformation history via R_0. The form (55)$_2$ highlights the evolving nature of β with temperature, strain and strain rate evolution. On this basis further remarks can be made as follows.

Remark 1. Under the modelling assumption, for plastic strain $p_2 > p_1$ close enough to consider that $T_1 \approx T_2 \approx T$, one can write from (55):

$$\beta(p_2,\dot{p},T) - \beta(p_1,\dot{p},T) \approx -\left[h'(p_2) - h'(p_1)\right]\frac{1}{R_0 + h'(p) + \Phi(p,\dot{p},T)} \tag{56}$$

Using the notation $\chi = \dfrac{1}{R_0 + h'(p) + \Phi(p,\dot{p},T)}$, with $\chi \geq 0$, relation (56) is reduced to

$$\frac{\partial \beta}{\partial p} \approx -\chi h''(p) \tag{57}$$

According to (57), it is possible to conclude that for material exhibiting strain hardening ($h''(p) > 0$), the inelastic heat fraction is decreasing with increasing strain, i.e. $\dfrac{\partial \beta}{\partial p} < 0$. On the contrary, for material exhibiting strain softening ($h''(p) < 0$), the inelastic heat fraction is increasing with increasing strain, i.e. $\dfrac{\partial \beta}{\partial p} > 0$.

Remark 2. According to $(55)_2$, $\beta(p, \dot{p}, T)$ is equal to unity when $h'(p) = 0$ which is satisfied for a perfectly plastic material (no strain hardening).

Application to fcc and bcc materials. The unified approach is now applied to fcc and bcc materials in the case of simple shearing such that $L_{ij} = \partial v_i / \partial x_j = 0$ except $L_{12} = \partial v_1 / \partial x_2 = \dot{\Gamma} \neq 0$. Material constants used for numerical simulations have been identified to reproduce Copper type material behaviour (see Voyiadjis & Abed, 2005, for experimental results) and Tantalum type material (see Voyiadjis & Abed, 2006, for experimental results) and are reported in Table 3.

	Copper (fcc)	Tantalum (bcc)
E (GPa)	120	170
ν	0.33	0.34
ρ_0 (kg/m³)	8930	16600
c_0 (J/kg.K)	380	140
T_m (K)	1350	3300
w	1/2	1/2
q	3/2	3/2
k/G_0 (K⁻¹)	4.9E-5	8E-5
$\dot{p}_0$ (s⁻¹)	1E10	1E9
R_0 (MPa)	100	100
R_∞ (MPa)	300	100
b	10	5
$\hat{\tau}_0$ (MPa)	X	1700

Table 3. Material constants for simple shearing simulation

The numerical evolution of stress invariant J_2, temperature T and inelastic heat fraction β is given versus shear strain $e_{12} = \gamma_{12}/2$ (the strain tensor **e** is obtained by time integration of the non objective strain rate tensor $\dot{\mathbf{e}}$, with $\dot{\mathbf{e}} = \mathbf{d} + \omega\mathbf{e} - \mathbf{e}\omega$) for various strain rates and initial temperatures considering Copper behaviour model in Fig.10 and Tantalum behaviour model in Fig.11. Adiabatic conditions are assumed for strain rates higher than 100 s⁻¹.

Figs.10a-11a show the increase of the flow stress with the increase of the strain rate whereas Figs.10d-11d show the increase of the flow stress with the decrease of the initial temperature. Fig.11a shows also the thermal softening induced in the flow stress of Tantalum while thermal softening is not significant in Fig.10a concerning Copper.

Values of numerical temperature in Fig.11b are very similar to those measured by (Kapoor & Nemat-Nasser, 1998) on Ta-2.5%W alloy under dynamic compression.

According to Figs.10c-10f and 11c-11f initial value of β is equal to 1 whatever the strain rate and the initial temperature. At large strain β converges to a value which depends on strain rate and initial temperature with a rate (negative according to remark 1) whose absolute value increases with decreasing strain rate and increasing initial temperature. The value for β at convergence is much smaller for Copper than for Tantalum.

Recent experimental investigations using fast response infrared optical device devoted to the measurement of heating during dynamic loading on Aluminium alloy (fcc) and steel (bcc) have shown that the inelastic heat fraction decreases with increasing strain (see

respectively Lerch at al., 2003, and Jovic et al., 2006). Unfortunately, time resolved data obtained with this type of reliable device are missing concerning Copper and Tantalum.
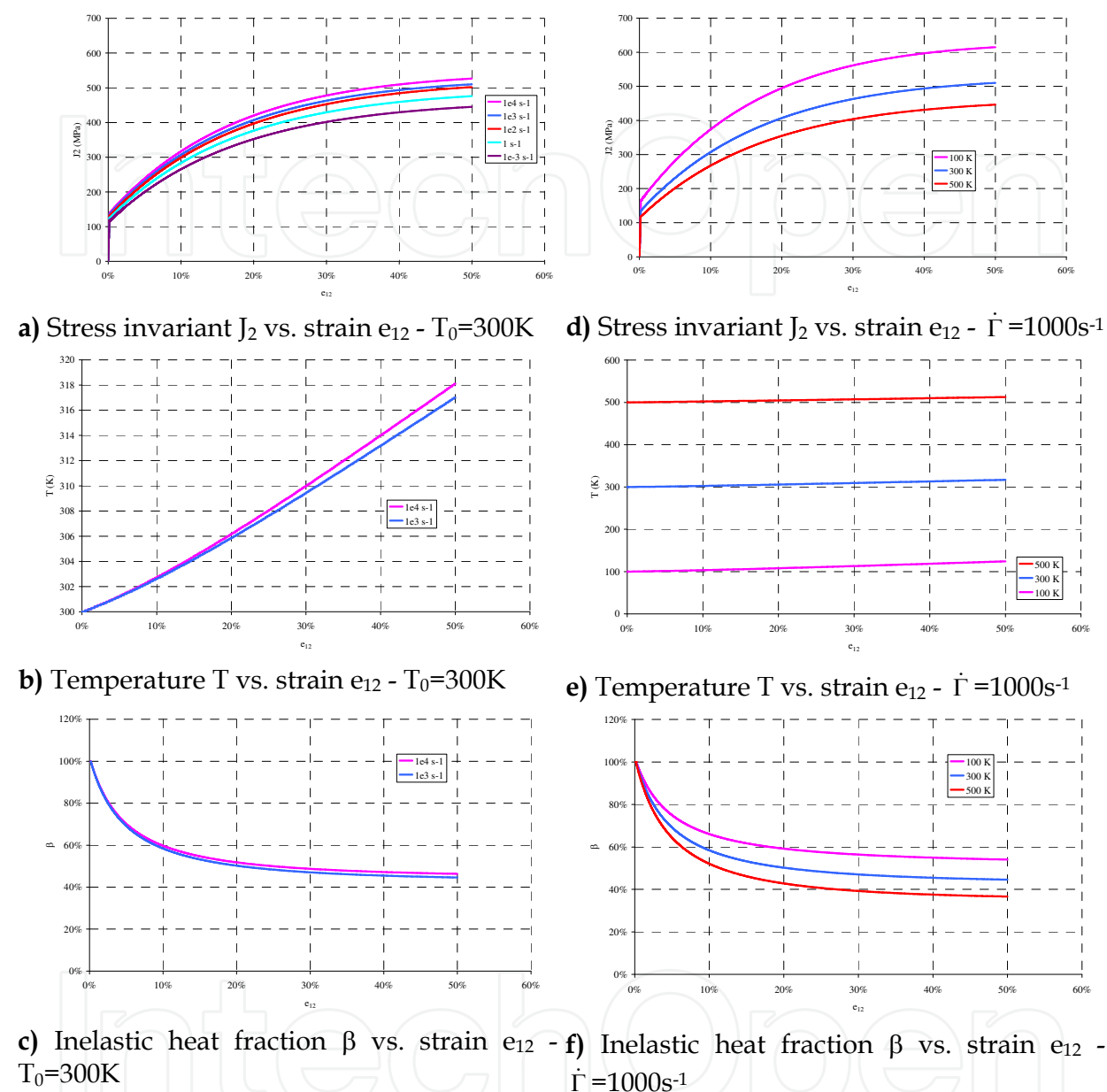
a) Stress invariant J_2 vs. strain e_{12} - T_0=300K

d) Stress invariant J_2 vs. strain e_{12} - $\dot{\Gamma}$ =1000s^{-1}

b) Temperature T vs. strain e_{12} - T_0=300K

e) Temperature T vs. strain e_{12} - $\dot{\Gamma}$ =1000s^{-1}

c) Inelastic heat fraction β vs. strain e_{12} - T_0=300K

f) Inelastic heat fraction β vs. strain e_{12} - $\dot{\Gamma}$ =1000s^{-1}

Fig. 10. Influence of shear strain rate and initial temperature on stress invariant and inelastic heat fraction. Adiabatic conditions are assumed for strain rates higher than 100 s^{-1}. Copper (fcc material).

5. Concluding remarks

The thermo-elastic/viscoplastic constitutive model, incorporating thermomechanical softening, ASB-induced degradation and anisotropy in the finite deformation framework, has the form favouring its adaptation for a large spectrum of metals and alloys susceptible to develop the ASB-related mechanism of deformation and failure under dynamic loading. As in any purpose-built constitutive model, some simplifications are introduced in the

model presented. They concern notably the strain hardening – limited to the isotropic one –, and the absence of the strain rate memory. However, the approach advanced brings in several novel potentialities. The principal one consists in the manner to account for ASB feedback effects, i.e. additional softening expressed via the strain hardening affinity (thermodynamic force) and furthermore in the manner to account for the ASB-induced plastic anisotropy in the yield function. At the same time, with regard to the absence of consensus concerning large elastic-plastic deformation including induced anisotropy, the particular kinematics developed in the model, based on the analogy between a band cluster and a macrodislocation, constitutes a physically motivated way (for the scale level considered) for a reasonable global description of thermomechanical consequences of ASB.

The model describes indeed most of salient effects while its modelling scale is based on a RVE much larger than the order of magnitude proper for the band's width. The deterioration internal variable introduced herein and its evolution capture principal singular features, notably the singular temperature growth, see also (Longère et al., 2005), where singular heating effects are quantified for a particular shock event. Another advantage concerns the three-dimensional formulation of the model, while many ASB-related studies and models regard fine description mostly limited to one-dimensional insight.

From the numerical standpoint (which is outlined here in the context of the application presented for a particular shock configuration for a ballistic penetration problem), there is no need to know *a priori* the band trajectory neither to refine finite element meshing for areas crossed by bands. For the ballistic penetration problem dealt with, the complex ASB-induced deterioration history is shown via numerical simulations presented. The plugging failure pattern is correctly issued, in accordance with projectile/plate geometry and shock configuration. Prospectively, there is a need to proceed with further numerical simulations for loading cases involving rotating principal stress directions and curved bands as observed, for example, in the experiments of Nesterenko et al. (1998). Thanks to the regularizing effects produced by material scale postulate, the double viscosity (viscoplasticity and viscous ASB-degradation), and an adaptive time step procedure, only slight mesh size dependence is observed in the post-localization (softening dominated) stages.

Regarding inelastic heat fraction study, a unified approach combining both concepts of dislocation mechanisms controlled by thermal activation and internal variable viscoplasticity for macroscopic modelling is considered in the present work. It is applied to strain, strain rate and temperature dependent metallic material behaviour in a range covering low velocity to moderately dynamic loading. Following the internal variable procedure and assuming the existence of thermodynamic potentials (free energy and dissipation potential), a consistent expression for the inelastic heat fraction is obtained. The corresponding form involves explicitly the influence of strain, strain rate and temperature as observed experimentally, and allows concluding that for a strain hardening model the inelastic heat fraction is decreasing with increasing strain. These theoretical results show the influence of the pertinent modelling – in terms of strain hardening/softening, thermal softening and strain rate dependence – on the inelastic heat fraction form and its highly evolving nature, notably for larger strain. Some models are actually intrinsically able to reproduce observed phenomena, pointedly the temperature rise induced by plastic deformation under adiabatic conditions, while others are not. The interest of satisfactory quantification of temperature rise in dynamic plasticity is evident. As shown e.g. by

Adiabatic Shear: Pre- and Post-critical Dynamic Plasticity Modelling
and Study of Impact Penetration. Heat Generation in this Context

259

Klepaczko & Resaig (1996), for adiabatic shear banding involving strain rates of about 10^5 s^{-1}, the increase in temperature for a class of bcc metals is close to the melting point.
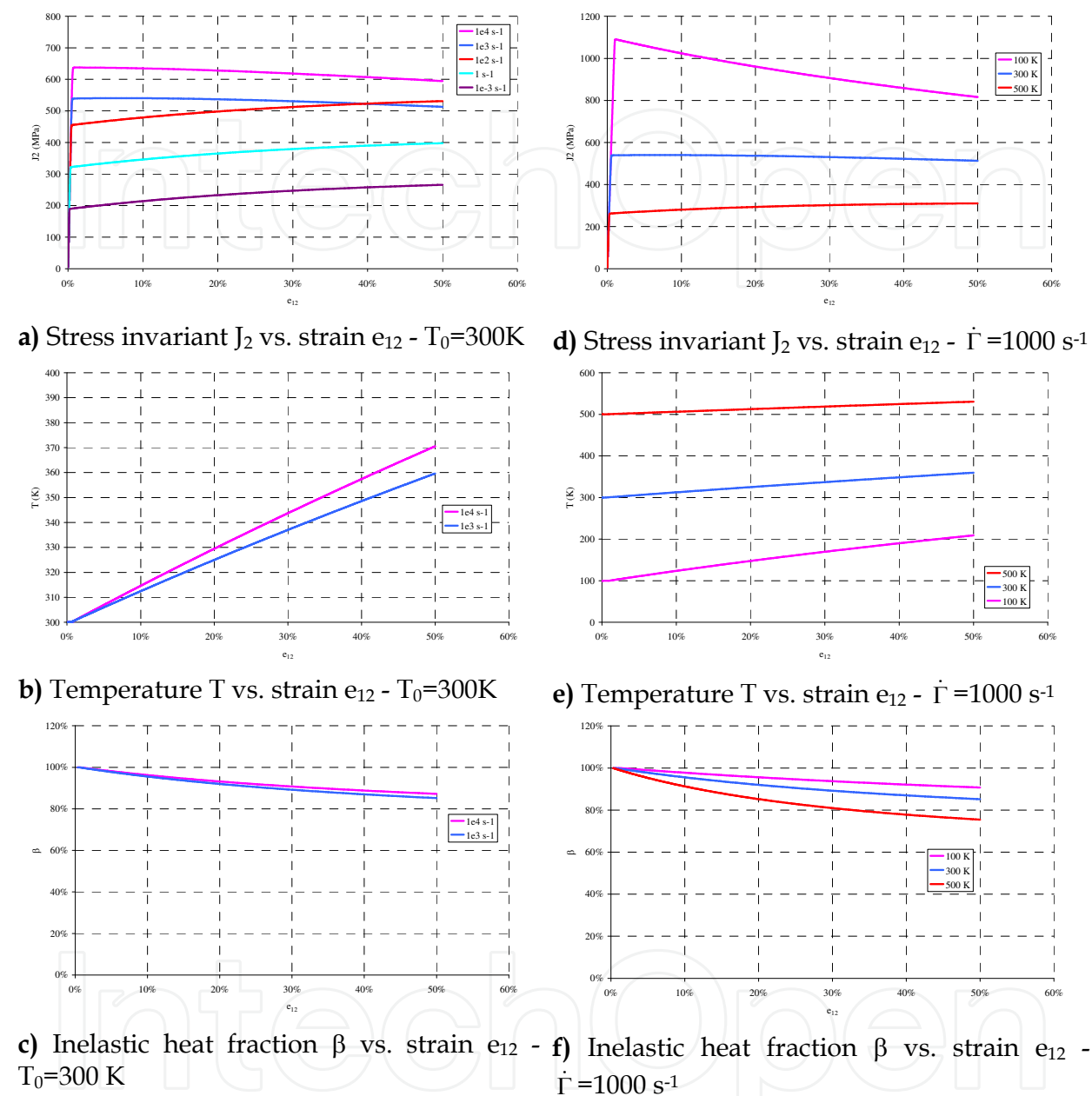

a) Stress invariant J_2 vs. strain e_{12} - T_0=300K

b) Temperature T vs. strain e_{12} - T_0=300K

c) Inelastic heat fraction β vs. strain e_{12} - T_0=300 K

d) Stress invariant J_2 vs. strain e_{12} - $\dot{\Gamma}$ =1000 s^{-1}

e) Temperature T vs. strain e_{12} - $\dot{\Gamma}$ =1000 s^{-1}

f) Inelastic heat fraction β vs. strain e_{12} - $\dot{\Gamma}$ =1000 s^{-1}

Fig. 11. Influence of shear strain rate and initial temperature on stress invariant and inelastic heat fraction. Adiabatic conditions are assumed for strain rates higher than 100 s^{-1}. Tantalum (bcc material)

6. References

Abu Al-Rub R.K. and Voyiadjis G.Z., 2006, A finite strain plastic-damage model for high velocity impact using combined viscosity and gradient localization limiters: Part I-Theoretical formulation, Int. J. Damage Mech., 15, 4, pp.293-334.

Aravas N., Kim K.S., Leckie F.A., 1990, On the calculations of the stored energy of cold work, J. Eng. Mat. Tech. (ASME), 112, pp.465-470.

Backman M.E. and Goldsmith W., 1978, The mechanics of penetration of projectiles into targets, Int. J. Engng Sci., 16, pp.1-99.

Bai Y.L., 1982, Thermo-plastic instability in simple shear, J. Mech. Phys. Solids, 30, 4, pp.195-207.

Bai Y.L. and Dodd B., 1992,.Adiabatic shear localisation, Oxford : Pergamon Press

Bataille J. and Kestin J., 1975, L'interprétation physique de la thermodynamique rationnelle, J. de Mécanique, 14, 2, pp.365-384.

Batra R.C. and Lear M.H., 2005, Adiabatic shear banding in plane strain tensile deformations of 11 thermoelastoviscoplastic materials with finite thermal wave speed, Int. J. Plast., 21, pp.1521-1545.

Børvik T., Hopperstad O.S., Berstad T. and Langseth M., 2001, Numerical simulation of plugging failure in ballistic penetration, Int. J. Solids Structures, 38, pp. 6241-6264.

Bronkhorst C.A., Cerreta E.K., Xue Q., Maudlin P.J., Mason T.A. and Gray III G.T., 2006, An experimental and numerical study of the localization behavior of tantalum and stainless steel, Int. J. Plast., 22, pp.1304-1335.

Burns T.J. and Davies M.A., 2002, On repeated adiabatic shear band formation during high speed machining, Int. J. Plast., 18, pp.487-506.

Camacho G.T. and Ortiz M., 1997, Adaptive Lagrangian modelling of ballistic penetration of metallic targets, Comput. Methods Appl. Mech. Engng, 142, pp.269-301.

Clifton R.J, Duffy J., Hartley K.A. and Shawki T.G., 1984, On critical conditions for shear band formation at high strain rates, Scripta Met., 18, pp.443-448.

Coleman B.D. and Gurtin M.E., 1967, Thermodynamics with internal state variables, J. Chem.-Phys., 47, pp.597-613.

Couque H., 2003a, A hydrodynamic hat specimen to investigate pressure and strain rate dependence on adiabatic shear band formation, J. Phys. IV, 110, pp.423-428.

Couque H., 2003b, Essais chapeau hydrodynamique d'un acier, GIAT Industries, Technical note DSAM/DT/MCP/3050.13.03C.

DeLuca E., Prifti J., Betheney W. and Chou S.C., 1998, Ballistic impact damage of S 2-glass-reinforced plastic structural armor, Composites Sc. Tech., 58, pp. 1453-1461.

Johnson G.R. and Cook W.H., 1983, A constitutive model and data for metals subjected to large strains, high strain rates and high temperatures, in Proceedings of the Seventh International Symposium on Ballistics, The Hague, The Netherlands, pp.541-547.

Jovic C., Wagner D., Hervé P., Gary G. and Lazzarotto L., 2006, Mechanical behaviour and temperature measurement during dynamic deformation on split Hopkinson bar of 304L stainless steel and 5754 aluminium alloy J. Phys. IV, 134, pp.1279-1285.

Kapoor R. and Nemat-Nasser S., 1998, Determination of temperature rise during high strain rate deformation, Mech. Mat., 27, pp.1-12.

Klepaczko J.R., 1994, Some results and new experimental technique in studies of adiabatic shear bands, Arch. Mech., 46, pp.201-229.

Klepaczko J.R. and Resaig B., 1996, A numerical study of adiabatic shear banding in mild steel by dislocation mechanics based constitutive relations, Mech. Mat., 24, pp.125-139.

Kulkarni M., Belytschko T. and Bayliss A., 1995, Stability and error analysis for time integrators applied to strain-softening materials, Comput. Methods Appl. Mech. Engng, 124, pp.335-363.

Adiabatic Shear: Pre- and Post-critical Dynamic Plasticity Modelling
and Study of Impact Penetration. Heat Generation in this Context
261

Lerch V., Gary G. and Hervé P., 2003, Thermomechanical properties of polycarbonate under dynamic loading, J. Phys. IV, 110, pp.159-164.

Liao S-C. and Duffy J., 1998, Adiabatic shear bands in a Ti-6Al-4V titanium alloy, J. Mech. Phys. Solids, 46, 11, pp.2201-2231.

Lodygowski T. and Perzyna P., 1997, Localized fracture in inelastic polycrystalline solids under dynamic loading processes, Int. J. Damage Mech., 6, pp. 364-407.

Longère P. and Dragon A., 2007, Adiabatic heat evaluation for dynamic plastic localization, J. Theor. Appl. Mech., 45, 2, pp.203-223.

Longère P. and Dragon A., 2008, Plastic work induced heating evaluation under dynamic conditions : critical assessment, Mech. Res. Com., 35, pp.135-141.

Longère P. and Dragon A., 2008, Evaluation of the inelastic heat fraction in the context of microstructure supported dynamic plasticity modelling, Int. J. Impact Eng., 35, 9, pp.992-999

Longère P. and Dragon A., 2009, Inelastic heat fraction evaluation for engineering problems involving dynamic plastic localization phenomena, J. Mech. Mat. Struct., 4, 2, pp.319-349.

Longère P., Dragon A. and Deprince X., 2009, Numerical study of impact penetration shearing employing finite strain viscoplasticity model incorporating adiabatic shear banding, J. Eng. Mat. Tech., ASME, 131, pp.011105.1-14.

Longère P., Dragon A., Trumel H. and Deprince X., 2005, Adiabatic shear banding induced degradation in a thermo-elastic/viscoplastic material under dynamic loading, Int. J. Impact Engng, 32, pp.285-320.

Longère P., Dragon A., Trumel H., de Resseguier T., Deprince X. and Petitpas E., 2003, Modelling adiabatic shear banding via damage mechanics approach, Arch. Mech., 55, pp.3-38.

Mahfuz H., Zhu Y., Haque A., Abutalib A., Vaidya U., Jeelani S., Gama B., Gillespie J. and Fink B., 2000, Investigation of high-velocity impact on integral armor using finite element method, Int. J. Impact Engng, 24, pp.203-217.

Marchand A. and Duffy J., 1988, An experimental study of the formation process of adiabatic shear bands in a structural steel, J. Mech. Phys. Solids, 36, 3, pp.251-283.

Martinez F., Murr L.E., Ramirez A., Lopez M.I. and Gaytan S.M., 2007, Dynamic deformation and adiabatic shear microstructures associated with ballistic plug formation and fracture in Ti-6Al-4V targets, Mat. Sc. Eng. A, 454-455, pp.581-589.

Mason J.J., Rosakis A.J. and Ravichandran G., 1994, On the strain and strain rate dependence of the fraction of plastic work converted to heat: an experimental study using high speed infrared detectors and the Kolsky bar, Mech. Mat., 17, pp.135-145.

Meixner J., 1969, Processes in simple thermodynamic materials, Arch. Rational Mech. Anal., 33, pp.33-53.

Molinari A., 1985, Instabilité thermoviscoplastique en cisaillement simple, J. Méca. Théorique et appliquée, 4, pp.659-684.

Molinari A., 1997, Collective behavior and spacing of adiabatic shear bands, J. Mech. Phys. Solids, 45, pp.1551-1575.

Molinari A. and Clifton R.J., 1987, Analytical characterization of shear localization in thermoviscoplastic materials, J. Appl. Mech., 54, 4, pp.806-812.

Molinari A., Musquar C. and Sutter G., 2002, Adiabatic shear banding in high speed machining of Ti-6Al-4V: experiments and modeling, Int. J. Plast., 18, 4, pp.443-459.

Nemat-Nasser S., LI Y. and Isaacs J.B., 1994, Experimental/computational evaluation of flow stress at high strain rates with application to adiabatic shear banding, Mech. Mat., 17, pp.111-134.

Nemat-Nasser S. and LI Y., 1998, Flow stress of f.c.c. polycrystals with application to OFHC Cu, Acta Mater., 46, 2, pp.565-577.

Nesterenko V.F., Meyers M.A. and Wright T.W., 1998, Self-organization in the initiation of adiabatic shear bands, Acta Mater., 46, 1, pp.327-340.

Pecherski R.B., 1998, Macroscopic effects of micro-shear banding in plasticity of metals, Acta Mech., 131, pp. 203-224.

Perzyna P., 1990, Influence of anisotropic effects on the micro-damage process in dissipative solids, in Yielding, Damage, and Failure of Anisotropic Solids, Ed. by J.P. Boehler, Mech. Engng Pub., pp. 483-507.

Recht R.F., 1964, Catastrophic thermoplastic shear, J. Appl. Mech., 31E, pp.189-193.

Rittel D., 1999, On the conversion of plastic work to heat during high strain rate deformation of glassy polymers, Mech. Mat., 31, pp.131-139.

Rittel D., 2009, Some comments on adiabatic shear localization, in Dynamic Behavior of Materials, Ed. A. Rusinek and P. Chevrier, pp.17-19.

Rittel D., Landau P. and Venkert A., 2008, Dynamic recrystallization as a potential cause for adiabatic shear failure, Phys. Rev. Letters, 101, 16, p.165501.

Rosakis P., Rosakis A.J., Ravichandran G. and Hodowany J., 2000, A thermodynamic internal variable model for the partition of plastic work into heat and stored energy in metals, J. Mech. Phys. Solids, 48, pp.581-607.

Sidoroff F. and Dogui A., 2001, Some issues about anisotropic elastic-plastic models at finite strain, Int. J. Solids Structures, 38, pp. 9569-9578.

Stevens J.B. and Batra R.C., 1998, Adiabatic shear bands in the Taylor impact test for a WHA rod, Int. J. Plast., 14, pp.841-854.

Suffis A., Lubrecht A.A. and Combescure A., 2003, A damage model with delay effect. Analytical and numerical studies of the evolution of the characteristic damage length, Int. J. Solids Structures, 40, pp. 3463-3476.

Taylor G.I. and Quinney H., 1934, The latent energy remaining in a metal after cold working, Proc. Roy. Soc., A413, pp.307-326.

Voyiadjis GZ. and Abed FH., 2005, Microstructural based models for bcc and fcc metals with temperature and strain rate dependency, Mech. Mat., 37, pp.355-378.

Voyiadjis GZ. and Abed FH., 2006, A coupled temperature and strain rate dependent yield function for dynamic deformations of bcc metals, Int. J. Plast., 22, pp.1398-1431.

Woodward R.L., 1990, Material failure at high strain rates, [in:] High velocity impact dynamics, J.A. Zukas [Ed.], John Wiley & Sons, pp.65-125.

Wright, 2002, The physics and mathematics of adiabatic shear bands, Cambridge University Press, Cambridge.

Zehnder A.T., 1991, A model for the heating due to plastic work, Mech. Res. Com., 18, 1, pp.23-28.

Zener C. and Hollomon J.H., 1944, Effect of strain rate upon plastic flow of steel, J. Appl. Phys., 15, pp.22-32.

Zerilli FJ. and Armstrong RW., 1987, Dislocation-mechanics-based constitutive relations for material dynamics calculations, J. Appl. Phys., 61, 5, pp.1816-1825.

Dynamic Modelling

Edited by Alisson V. Brito

When talking about modelling it is natural to talk about simulation. Simulation is the imitation of the operation of a real-world process or systems over time. The objective is to generate a history of the model and the observation of that history helps us understand how the real-world system works, not necessarily involving the real-world into this process. A system (or process) model takes the form of a set of assumptions concerning its operation. In a model mathematical and logical assumptions are considered, and entities and their relationship are delimited. The objective of a model – and its respective simulation – is to answer a vast number of "what-if" questions. Some questions answered in this book are: What if the power distribution system does not work as expected? What if the produced ships were not able to transport all the demanded containers through the Yangtze River in China? And, what if an installed wind farm does not produce the expected amount of energyt? Answering these questions without a dynamic simulation model could be extremely expensive or even impossible in some cases and this book aims to present possible solutions to these problems.

How to reference

In order to correctly reference this scholarly work, feel free to copy and paste the following:

Patrice Longère and André Dragon (2010). Adiabatic Shear: Pre- and Post-Critical Dynamic Plasticity Modelling and Study of Impact Penetration. Heat Generation in this Context, Dynamic Modelling, Alisson V. Brito (Ed.), ISBN: 978-953-7619-68-8, InTech, Available from: http://www.intechopen.com/books/dynamic-modelling/adiabatic-shear-pre-and-post-critical-dynamic-plasticity-modelling-and-study-of-impact-penetration-h

INTECH
open science | open minds